5-7-2024

Molecular Therapy and Nucleic Acid Adeno-Associated Virus-Based Gene Therapy Delivering Combinations of Two Growth-Associated Genes to MPS IVA Mice

Estera Rintz

Betul Celik

Nidhi Fnu

Angélica María Herreño-Pachón

Shaukat Khan

See next page for additional authors

Authors

Estera Rintz, Betul Celik, Nidhi Fnu, Angélica María Herreño-Pachón, Shaukat Khan, Shunji Tomatsu, and Eliana Benincore-Flórez

Molecular Therapy
Nucleic Acids
Original Article

Adeno-associated virus-based gene therapy delivering combinations of two growth-associated genes to MPS IVA mice

Estera Rintz,[1,2] Betul Celik,[1,3] Nidhi Fnu,[1,3] Angélica María Herreño-Pachón,[1,3] Shaukat Khan,[1,4] Eliana Benincore-Flórez,[1] and Shunji Tomatsu[1,3,4]

[1]Nemours Children's Health, Wilmington, DE 19803, USA; [2]Department of Molecular Biology, Faculty of Biology, University of Gdansk, 80-308 Gdansk, Poland; [3]Faculty of Arts and Sciences, University of Delaware, Newark, DE 19716, USA; [4]Department of Pediatrics, Thomas Jefferson University, Philadelphia, PA 19144, USA

Mucopolysaccharidosis type IVA (MPS IVA) is caused by a deficiency of the galactosamine (N-acetyl)-6-sulfatase (GALNS) enzyme responsible for the degradation of specific glycosaminoglycans (GAGs). The progressive accumulation of GAGs leads to various skeletal abnormalities (short stature, hypoplasia, tracheal obstruction) and several symptoms in other organs. To date, no treatment is effective for patients with bone abnormalities. To improve bone pathology, we propose a novel combination treatment with the adeno-associated virus (AAV) vectors expressing GALNS enzyme and a natriuretic peptide C (CNP; NPPC gene) as a growth-promoting agent for MPS IVA. In this study, an MPS IVA mouse model was treated with an AAV vector expressing GALNS combined with another AAV vector expressing NPPC gene, followed for 12 weeks. After the combination therapy, bone growth in mice was induced with increased enzyme activity in tissues (bone, liver, heart, lung) and plasma. Moreover, there were significant changes in bone morphology in CNP-treated mice with increased CNP activity in plasma. Delivering combinations of CNP and GALNS gene therapies enhanced bone growth in MPS IVA mice more than in GALNS gene therapy alone. Enzyme expression therapy alone fails to reach the bone growth region; our results indicate that combining it with CNP offers a potential alternative.

INTRODUCTION

The mucopolysaccharidoses (MPS) are a group of rare inherited lysosomal storage disorders with a total incidence of 1 in 25,000 births.[1] The low incidence of MPS is also caused by the poor prenatal and birth diagnosis of the patients.[2] MPS group is classified into eight types based on the defective enzyme in the lysosome.[3,4] When a lysosomal enzyme is defective, it loses its ability to efficiently break down its enzyme substrates, glycosaminoglycans (GAGs). As a result, GAGs build up inside the cell and throughout the entire organism. The symptoms of MPS vary depending on the specific type of the disorder, the defective enzyme, and the accumulated specific GAGs.[3]

Most symptoms are connected to the GAG accumulation within the body, such as organomegaly, heart dysfunction, hernias, and neurological and skeletal symptoms.[3] Currently, there is no cure for MPS. Treatment options for the MPS include enzyme replacement therapy (ERT) and hematopoietic stem cell transplantation (HSCT). ERT has several limitations: high cost, immune response, weekly administration, and ineffectiveness for bone and brain treatment. HSCT has the limitations of finding a suitable donor, transplant rejection, transplant age limits, invasive procedures, limited correction of the CNS, and skeletal symptoms.[5,6] Additionally, patients need constant supportive or palliative care that includes rehabilitation, surgical interventions, or medications that can control musculoskeletal, respiratory, ophthalmological, and neurological manifestations.[7]

The most severe symptoms of MPS occur when there is dysfunction in the CNS or skeletal abnormalities.[8] Novel therapies primarily targeting the CNS are under clinical or preclinical studies and will be available to patients soon. These therapies include receptor-mediated transport of the enzyme (RMT)[9] or gene therapy.[10] RMT is the direct enzyme modification that targets specific receptors, helping to transport ligands through barriers such as blood-brain barrier. RMT therapy was assessed in several MPS types: MPS I,[11–13] MPS II,[14,15] MPS III,[16,17] and MPS VII.[18] Some of these therapies are approved or in clinics: MPS I (NCT04227600, NCT03053089, NCT02371226) and MPS II (NCT04573023, NCT04251026) (Database: ClinicalTrials.gov). Similarly, our study used a receptor-based approach targeting natriuretic peptide C (CNP) receptors with CNP, which induces bone growth. Gene therapy is extensively studied for MPS patients. It can be distinguished into two main categories depending on the way of vector administration: *in vivo* and *ex vivo* gene therapy. *In vivo* gene therapy is a direct transfer of the viral vector to the organism; it can be through intravenous, intracerebral, or other direct administration routes. *Ex vivo* gene therapy includes more steps: collecting the cells from patients (e.g., stem cells), transduction with the vector of interest, and re-administration of the transduced cells to the patient.[10] Both approaches are studied

Received 13 February 2024; accepted 3 May 2024;
https://doi.org/10.1016/j.omtn.2024.102211.

Correspondence: Shunji Tomatsu, Nemours Children's Health, Wilmington, DE 19803, USA.
E-mail: shunji.tomatsu@nemours.org

for the MPS patients in clinics (Table S1). Most potential gene therapies focus on the cross-correction mechanism of the enzyme in the blood flow. The enzyme is expressed in the cell of interest and secreted through the bloodstream to other cells in the body. High expression of the enzyme from viral vector helps to reach hard-to-treat tissues, such as brain or bone.[19] However, elevated transgene expression could potentially impact the organism, leading to a heightened immune response.

Available treatments for MPS can help to manage specific symptoms and extend life expectancy.[20] However, individuals with MPS still experience significant challenges due to skeletal abnormalities, including kyphosis, scoliosis, genu valgum, trachea obstruction, joint pain, and severe short stature. Additional therapeutic approaches are needed to address skeletal dysfunction in these disorders, including inflammation reduction and pain management.[21,22]

The type of accumulated GAGs in the bones determines the specific cells affected. In MPS types I, II, and VI, dermatan sulfate accumulates mostly in bone cells like osteocytes, osteoblasts, and osteoclasts, leading to an imbalance in bone formation. Imbalances in bone formation can result in abnormal bone ossification, growth, and strength, with a consequent risk of osteoporosis.[23–25] In MPS IVA (Morquio A syndrome), keratan sulfate (KS) accumulates mainly in the bone cartilage. Targeting chondrocyte cells, responsible for cartilage formation in avascular regions of the bone, poses significant challenges in treatment.[26] Consequently, additional treatment approaches are necessary to address avascular cartilage tissue and alleviate the burden of skeletal-related symptoms in MPS IVA patients.

Numerous investigations utilize adeno-associated virus (AAV) vectors in bone research, both for delivering a transgene of interest[27–29] and in more recent studies employing AAV vectors for base editing in the treatment of bone fragility.[30] Our prior studies have demonstrated the effectiveness of AAV vectors expressing the galactosamine (N-acetyl)-6-sulfatase (GALNS) enzyme in treating MPS IVA in the mouse model.[31,32] Our analysis revealed increased enzyme activity and decreased chondrocyte volume due to a cross-correction mechanism.[32] However, we did not observe an increased proliferation of chondrocytes. Thus, to address the bone, we used an AAV8 vector expressing the peptide that previously showed bone growth induction in the MPS IVA mice.[33] CNP, a potential bone-penetrating agent, stimulates bone growth by activating the natriuretic peptide receptor B on chondrocytes. Despite its therapeutic promise for skeletal dysplasia, the short half-life of natural CNP and the need for repeated injections of modified CNP currently limit its effectiveness. Our previous results showed that CNP effectively targets chondrocytes, activating its proliferation and differentiation in the growth plate of MPS IVA mice.[33]

In this article, our objective was to evaluate a combined therapy in a mouse model of MPS IVA. This therapeutic strategy involved gene therapy applying two different transgenes.

We focused on two primary issues observed in MPS IVA patients: KS and C6S accumulation and bone growth failure. To achieve this goal, we administered AAV vectors co-expressing two transgenes, the GALNS enzyme and the bone growth-inducing peptide, CNP. AAV9 has a broader targeting range within the body, affecting tissues such as striated muscles, liver, bone, and the CNS, potentially leading to greater expression of the vector; thus, we used this serotype for GALNS expression.[34–37] AAV8 also has a broad range of targeted tissues when delivered locally,[38–43] with the greatest transduction efficacy in hepatocytes out of all AAV serotypes in different models.[37,38] Considering our familiarity with AAV vectors, we opted for AAV8 as the expression vector for CNP, which will be expressed more in liver. This choice was made to prevent potential overexpression in one particular tissue. Also, we avoided antibodies against one specific serotype raised, causing more immune reactions and adverse effects. Our experiments highlight the significance of carefully controlling the dosage of CNP to avoid unintended immune reactions.

RESULTS

Growth induction in MPS IVA by combination therapy is dose dependent

To establish the effects of combination therapy gene therapy with CNP and GALNS enzyme on the MPS IVA mouse model, we injected intravenously vectors according to Figure 1 under housekeeping promoter CAG into 4-week-old mice.

Mice were measured weekly for weight and length (nose to tail and nose to anus). Additionally, pictures were obtained on the autopsy day to observe physiological differences (anatomical) among treated mice (Figure 2A). The body weights of MPS IVA and wild-type (WT) mice were significantly different only at week 4 (Figure 2B). In the combination therapy, we observed a difference only in group 7 treated with two vectors AAV9-hGALNS and AAV8-hNPPC (dose 4×10^{13} GC/kg + 4×10^{13} GC/kg) starting from week 4 in comparison to WT mice and at weeks 9, 10, and 12 in comparison with the untreated MPS IVA mice. Weight differences were insignificant in any other groups during the experiment. We measured growth patterns in all experimental groups weekly. There was no difference between untreated MPS IVA and WT groups. During the experiment, mice in groups 5–7 were injected with two vectors (*NPPC* and *GALNS*) separately, and mice in group 4 received dual AAV vectors with two tandem genes (Figures 2C and 2D). There was no difference in growth parameters in the group injected with only the AAV9-hGALNS vector compared with the WT or untreated MPS IVA mouse group. We saw significant differences between groups in the growth pattern. Mice in group 7 were treated with two vectors, AAV9-hGALNS and AAV8-hNPPC (dose 4×10^{13} GC/kg + 4×10^{13} GC/kg), which had the highest dose of CNP and their rapid growth pattern. The difference was significant in the first week after the injection, with more than 2 cm in both measurements (nose to tail and nose to anus) compared with the WT and MPS IVA mice. Growth was stabilized around week 11; however, mice started to have abnormal motion and were terminated at week 13. Due to overgrowth, we decreased the dose of the injected AAV8-NPPC in the next groups. Mice injected with the lowest dose of the CNP-expressing vector showed slight differences in weeks 7 and 9–12; we did not

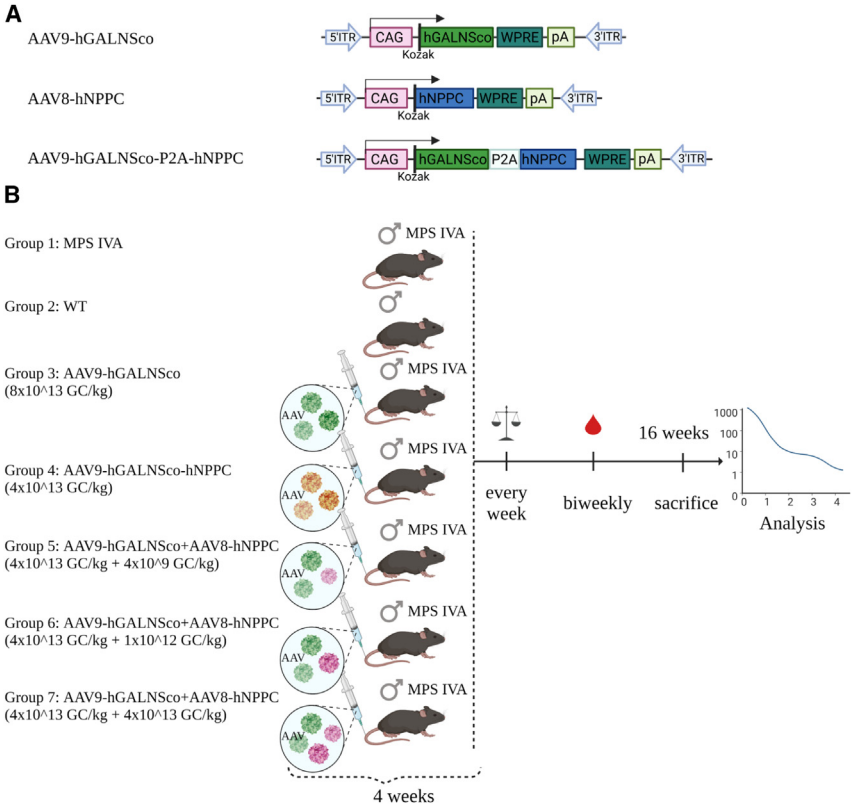

Figure 1. Experimental design

(A) An AAV vector construct. We used three AAV vectors containing synthetic ubiquitous CAG promoter. (B) Experiments started at 4 weeks of age. We have seven experimental groups: (1) untreated MPS IVA; (2) WT control (WT); (3) MPS IVA mice AAV9 vector expressing human GALNS enzyme (AAV9-hGALNS); (4) MPS IVA mice AAV9 vector expressing two transgenes-human GALNS enzyme and human CNP (AAV9-hGALNSco-hNPPC); and three groups (5, 6, and 7) of combination therapy with the same vectors with different dosage (AAV9-hGALNS+ AAV8-hNPPC). During the experiments, mice were measured weekly for body weight, nose-tail length, and nose-anus length, with biweekly blood collection. Mice were euthanized at 16 weeks (except group 7, which was euthanized at 13 weeks). After that, the analysis was undertaken. This figure was prepared using BioRender.com.

see a difference in growth pattern in the other weeks. As the difference in the lowest dose was minimal in comparison with WT and MPS IVA mice, we administered the middle dose of the AAV8-NPPC injected with two vectors AAV9-hGALNS and AAV8-hNPPC (dose 4×10^{13} GC/kg + 1×10^{12} GC/kg) (group 6). In group 6, we saw a significant difference in the growth pattern, starting at week 5 and stabilizing at week 9. Group 4, with two tandem transgenes, showed a higher growth pattern than group 7. In group 4, the difference in growth started at week 7 compared with WT and MPS IVA mice.

AAV9-hGALNS delivery increases GALNS activity

Before performing *in vivo* experiments, we evaluated the transduction efficacy of the AAV9-hGALNS vector in human fibroblast cell lines (either healthy or MPS IVA patients). At 48 h after transduction with the vector, we saw an elevation of the GALNS enzyme activity in MPS IVA patient's cell lines using a multiplicity of infection (MOI) (10^5 and 10^6). We did not see a difference in the enzyme activity between MOIs, and neither MOI reached the activity level of cells from healthy individuals (Figure S1). Therefore, we used a high dose of AAV9-hGALNS in a mouse model of MPS IVA. The mouse model used in this study was the MPS IVA knockout mice (MKC2; C57BL/6 background), as described previously.[33] These mice lack GALNS enzyme activity, resulting in the accumulation of storage material (KS) in various tissues and plasma. These biomarkers (enzyme activity and substrate accumulation) were extensively used to assess the severity of the phenotype and measure the effectiveness of various therapeutic approaches in MPS IVA patients and animal models.[44–47] We collected several tissues (liver, bone, trachea, muscle, spleen, heart, lung, eye, thymus, and brain) (Figure 3A) to evaluate the enzyme activity. Additionally, we evaluated plasma GALNS enzyme activity every other week to see the progression of the therapy (Figure 3B). We saw increased GALNS enzyme activity in tissues collected in all treated groups. In group 3, which was treated with only AAV9-hGALNSco, we saw a supraphysiological level of GALNS enzyme activity in every tissue, except trachea and brain. Plasma enzyme activity showed increased expression starting from week 6 and gradually increased until week 16. Group 4, which was treated with dual AAV vector expressing tandem genes, GALNS and CNP, showed that the enzyme activities in liver and heart were similar to those of WT; in other tissues, the activity was either not detected or was on the lower level. Plasma enzyme activity in group 4 was not detected during the experiment. Combination therapy of two separately injected vectors (groups 5–7) showed that the GALNS activity exceeded WT expression in all tissues except trachea and brain. The same pattern was seen in the plasma GALNS activity.

Additionally, we quantified the GALNS protein by western blot to evaluate the possible outcome of lower enzyme activity in group 4 injected with AAV9-hGALNS-hNPPC. We saw a higher level of liver GALNS protein in group 4 compared with WT mice, consistent with the enzyme activity (Figure 4A). All groups had significantly higher GALNS protein levels than the WT mouse group. As the protein concentration and enzyme activity were synchronized, we also measured anti-GALNS antibodies in the final week (Figure 4B). Based on our previous results,[31] we anticipated an increase in antibody levels throughout the weeks of the experiment, peaking around the final weeks. Therefore, we drew our conclusions on the antibody levels from the final week, correlating them with the enzyme activity. In group 4, no GALNS enzyme activity was seen in plasma

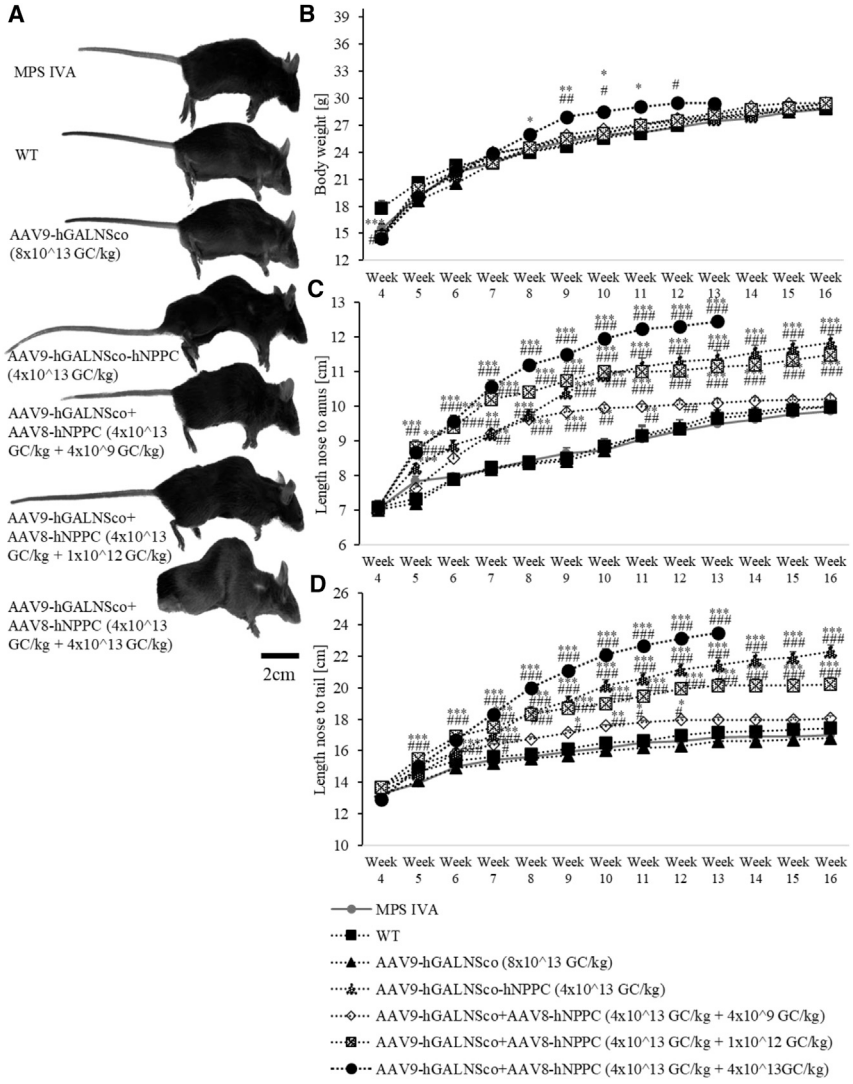

Figure 2. Dose-dependent growth induction in MPS IVA mice

Seven experimental groups are presented: (1) untreated MPS IVA; (2) WT control (WT); (3) MPS IVA mice AAV9 vector expressing human GALNS enzyme (AAV9-hGALNS); (4) MPS IVA mice AAV9 vector expressing two transgenes-human GALNS enzyme and human CNP (AAV9-hGALNSco-hNPPC); and three groups (5, 6, and 7) of combination therapy with the same vectors with different dosages (AAV9-hGALNS+ AAV8-hNPPC). (A) Picture of mice on the day week of the experiment. (B) Body weight of mice during the experiment. (C) Body length measurement from nose to anus of mice during the experiment. (D) Body length measurement from nose to tail of mice during the experiment. Results are shown as mean values ± SEM (n = 5). The following statistical symbols were used to denote the following vs. WT group, ***p ≤ 0.001, **p ≤ 0.01, *p ≤ 0.05; vs. untreated MPS IVA group, ###p ≤ 0.001, ##p ≤ 0.01, #p ≤ 0.05.

throughout all the checkpoints (weeks 4–16), while we saw the highest anti-GALNS antibodies in the final week. Moreover, even though group 7 had high antibodies, the expression of the GALNS was high enough not to clear the enzyme from the bloodstream.

GAGs in blood and tissues decreased as a result of AAV-GALNS delivery

To measure the effectiveness of the AAV vector therapy at autopsy, we measured mono-sulfated KS, the major KS component, and dermatan sulfate (DS; Di4S) in both plasma and tissues (liver, bone, heart, and lung). The levels of these two GAGs are shown in Figure 5. KS was accumulated in plasma and all tissues except the heart (Figure 5A) of the MPS IVA mouse model. After treatment with any vector, we saw a decrease in KS levels in plasma and all tissues except heart. We saw the accumulation of the DS only in liver samples of MPS IVA compared with the WT mice (Figure 5B). After treatment with any vector, we saw decreased Di4S (DS) accumulation in the liver. We did not detect differences in bone samples. Additionally, we measured the level of other GAGs in the tissues and plasma: *O*-sulfated heparan sulfate (DiHS-0S) and *N*-sulfated heparan sulfate (DiHS-NS) (Figure S2). We did not observe significant differences between the MPS IVA and WT mice in the measured GAGs. For the DiHS-0S (Figure S2B), we only saw an increase in plasma for groups 6 and 7 compared with both WT and MPS IVA mice. The only increase in the DiHS-NS (Figure S2C) was in groups 6 and 7 in lungs.

AAV vector biodistribution and expression

To establish the biodistribution of the vectors, we performed digital PCR (dPCR) in bone and liver during the study (Figure 6). Both vectors (expressing human *GALNS* and *NPPC*) were undetected in bone and liver in WT and untreated MPS IVA groups. GALNS was detected in all groups in both bone (Figure 6A) and liver (Figure 6B). The highest vector copy number for the *GALNS* was detected in group 3, which was injected with only the AAV9-hGALNS vector in bone; other groups had similar copy numbers. In the case of *NPPC*, the biodistribution of the dual vector with two transgenes (group 4) was the highest in both bone and liver (Figures 6C and 6D) compared with other groups. For the vector with the lowest dose of NPPC (group 5), the NPPC vector was undetectable in both bone and liver. In the middle dose (group 6), it was undetectable in bone and with minimal detection in liver (Figures 6C and 6D). In the highest dose of combination therapy (group 7), the NPPC vector was detected in both bone and liver, but it was lower than in group 5 (Figures 6C and 6D).

Additionally, we measured the plasma level of human NT-proCNP as a marker of CNP expression (Figure 6E). Human NT-proCNP was

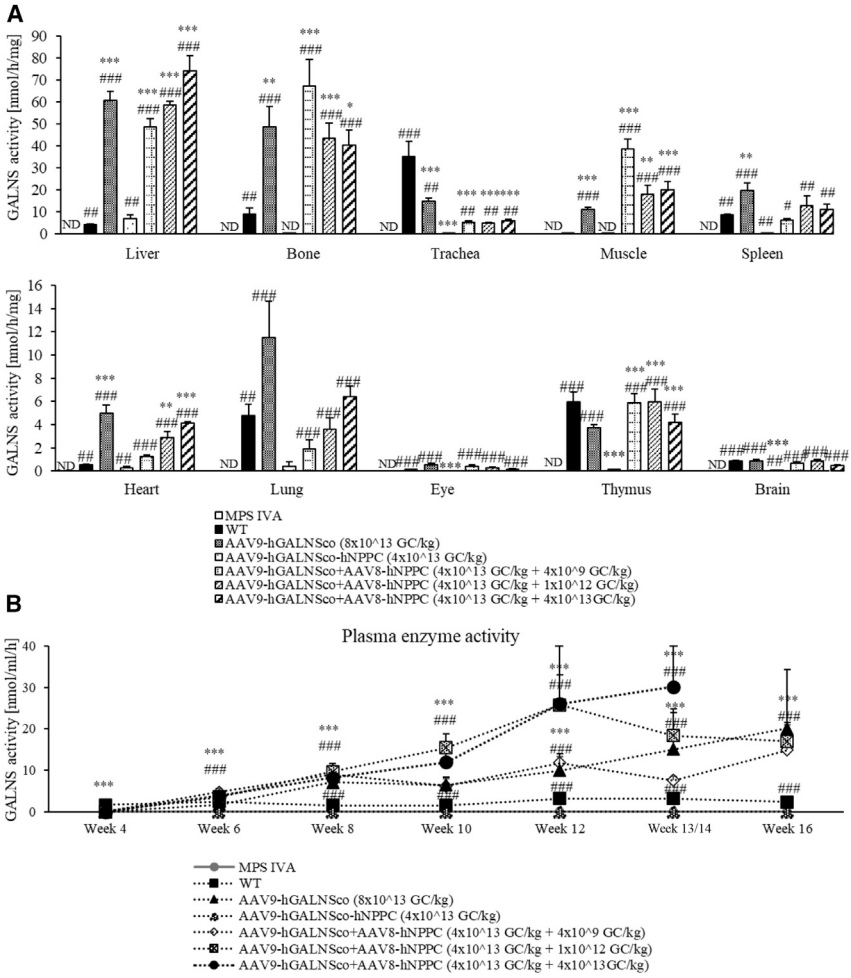

Figure 3. GALNS enzyme activity in MPS IVA mice treated with AAV9-hGALNS vector

Seven experimental groups are presented: (1) untreated MPS IVA; (2) WT control (WT); (3)MPS IVA mice AAV9 vector expressing human GALNS enzyme (AAV9-hGALNS); (4) MPS IVA mice AAV9 vector expressing two transgenes-human GALNS enzyme and human CNP (AAV9-hGALNSco-hNPPC); and three groups (5, 6, and 7) of combination therapy with the same vectors with different dosages (AAV9-hGALNS+ AAV8-hNPPC). (A) GALNS activity in tissues (liver, bone, trachea, muscle, spleen, heart, lung, eye, thymus, and brain). (B) Plasma GALNS activity during the experiment. The figure represents week 13/14 because group 7 was terminated in week 13, while other groups had blood collected at week 14. Results are shown as mean values ± SEM (n = 5). The following statistical symbols were used to denote the following vs. WT group, ***p ≤ 0.001, **p ≤ 0.01, *p ≤ 0.05; vs. untreated MPS IVA group, ###p ≤ 0.001, ##p ≤ 0.01, #p ≤ 0.05.

detected at the highest level in group 7 in comparison with other groups. It was undetectable in group 5, and minimal detection was observed in group 4 injected with two transgenes (Figure 6E).

We performed immunohistochemistry staining to investigate the presence of the GALNS enzyme in the bone growth plate (Figure S3). The expression of GALNS in WT and AAV9-hGALNSco was on the same level. We did not detect any bone GALNS expression in the AAV9-hGALNSco-hNPPC vector. In the combination therapy group, the GALNS expression level was similar to the highest expression in the bone marrow region of the bone (Figures S3E–S3G).

Micro-computed tomography

We analyzed cortical and trabecular bone structure by using micro-computed tomography (micro-CT). Micro-CT created a 3D representation of the specimen using X-ray attenuation data, enabling direct measurements of bone morphology. We used micro-CT to examine bone morphometry in seven experimental groups, focusing on both trabecular and cortical bone (Figure 7). We did not see significant differences between WT and untreated MPS IVA mice. Treatment with AAV9-hGALNSco significantly increased trabecular separation (Figure 7E), compared with WT and MPS IVA mice. AAV9-hGALNSco-hNPPC and AAV9-hGALNSco+AAV8-hNPPC (group 5) treatments were not significantly different, while treatment with AAV9-hGALNSco+AAV8-hNPPC (group 6) increased bone area (Figure 7J) and cortical thickness (Figure 7N) compared with both WT and MPS IVA. In group 7 with a high dose of combination therapy, an increase of values was seen in trabecular volume of interest (Figure 7A), total area (Figure 7I), and medullary area (Figure 7L), while a decrease was seen in the percent bone volume (Figure 7C), trabecular thickness (Figure 7F), bone mineral density (Figure 7G), BA/TA (Figure 7K), and cortical thickness (Figure 7N).

Induction of chondrocyte proliferation

Knee joint lesions were assessed using toluidine blue staining 12 weeks after the administration of AAV vectors in MPS IVA mice. In untreated MPS IVA mice, GAG storage vacuoles were observed in the growth plate and articular cartilage of the tibia (Figure 8), as well as in the articular disc and growth plate of femur and meniscus region (Figures S5 and S6). The growth plate region was also disorganized, characterized by chondrocytes with vacuolation (Figures 8 and S4–S6).

We evaluated the improvement of vacuoles and disorganized column structures in knee joints of MPS IVA mice using pathological scores, which showed a tendency of improvement in MPS IVA mice treated with the combination therapy of AAV vector expressing GALNS and CNP compared with untreated mice. The pathological score of MPS IVA mice treated with groups AAV9-hGALNSco+AAV8-hNPPC

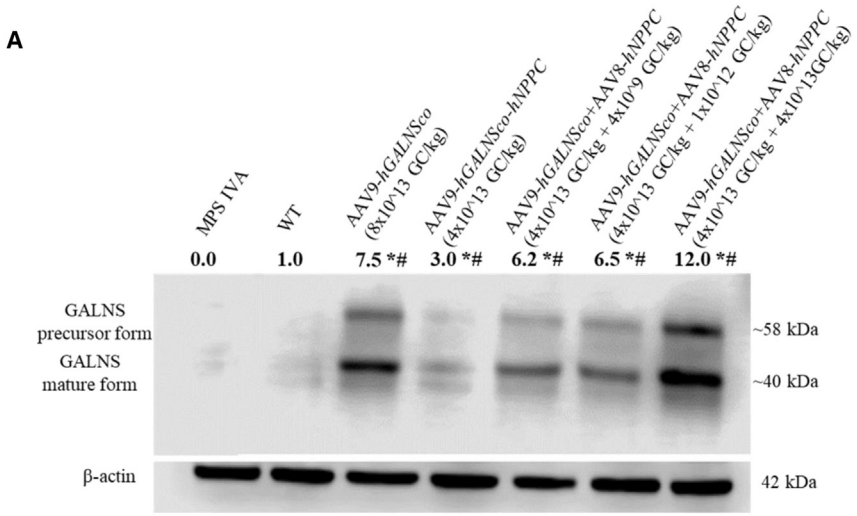

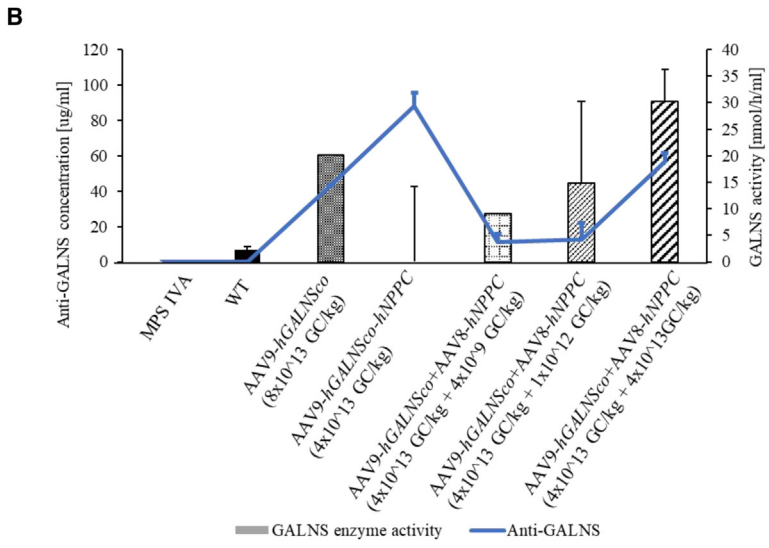

Figure 4. GALNS expression and anti-GALNS antibodies

Seven experimental groups are presented: (1) untreated MPS IVA; (2) WT control (WT); (3) MPS IVA mice AAV9 vector expressing human GALNS enzyme (AAV9-hGALNS); (4) MPS IVA mice AAV9 vector expressing two transgenes-human GALNS enzyme and human CNP (AAV9-hGALNSco-hNPPC); and three groups (5, 6, and 7) of combination therapy with the same vectors with different dosages (AAV9-hGALNS+ AAV8-hNPPC). (A) Liver GALNS protein level measured by western blot; calculated analysis of the mature form of the GALNS protein. (B) Correlation of plasma enzyme activity with GALNS clearance antibodies. Results are shown as mean values ± SEM (n = 5). The following statistical symbols were used to denote the following vs. WT group, $^{*}p \leq 0.001$; vs. untreated MPS IVA group, #p ≤ 0.001.

(groups 6 and 7) was significantly lower for the column structure of chondrocytes in the growth plate area of tibia and femur bone compared with those treated with MPSIVA, but not as low as the WT level (as shown in Table 1). The vacuolization of chondrocytes in the articular cartilage area was compared with those treated with MPSIVA. The WT level was lower than in the treated groups (groups 6 and 7). The column structure of chondrocytes in the articular cartilage area of tibia was improved after combination treatment AAV9-hGALNSco+AAV8-hNPPC (groups 5, 6, and 7), as well as in the AAV9-hGALNSco (group 3) alone. However, a notably lower score compared with untreated MPS IVA was explicitly observed in the columnar structure of chondrocytes within the articular cartilage region of the femur. This effect was evident only after treatment with a higher dose of CNP in the combination therapy AAV9-hGALNSco+AAV8-hNPPC (group 7). Regarding the vacuolization of chondrocytes in the ligament area, the score in two groups, AAV9-hGALNSco + AAV8-hNPPC (groups 6 and 7), was lower than in the untreated MPS IVA group. None of the treatments reached the WT level in the score pathology analysis.

DISCUSSION

MPS IVA exerts its most profound impact on the skeletal system, leading to skeletal dysplasia and restricted endurance. This dysplasia significantly decreases mobility and often necessitates multiple surgeries on the hip, legs, trachea, and spine. During the lifetime of the patients, the length of the trachea outgrows skeletal growth, leading to airway obstruction, one of the most life-threatening conditions for the patients.[48–50] Therapeutic interventions in patients address skeletal (mostly surgeries) and non-skeletal symptoms (ERT and HSCT). ERT improved endurance, lung capacity, and walking ability.[51] Nevertheless, long-term evaluations have shown that pulmonary function decreased over time.[51] Even when patients received ERT before 2 years of age, their growth did not improve.[52] MPS IVA patients also face life-threatening cardiovascular issues, leading to high morbidity and mortality. In MPS IVA, the small size of the left ventricle decreases stroke volume and increases heart rate, while impaired diastolic filling arises from thickened left ventricle and heart valves. After ERT, cardiovascular function did not change for older patients.[51] Early implementation of ERT stabilizes cardiac hypertrophy, but valvular heart disease may take several years to stabilize.[53] ERT for MPS IVA patients decreases KS levels (decreased organomegaly) and improves endurance; however, it has a minor to no effect on the skeletal, pulmonary, and cardiac problems attributed to a considerable part of the mortality rate in MPS IVA patients.[54] HSCT showed better improvement than ERT in skeletal abnormalities. Ten years after transplantation, patients showed a decreased need for surgical intervention and delayed progression of skeletal dysmorphia.

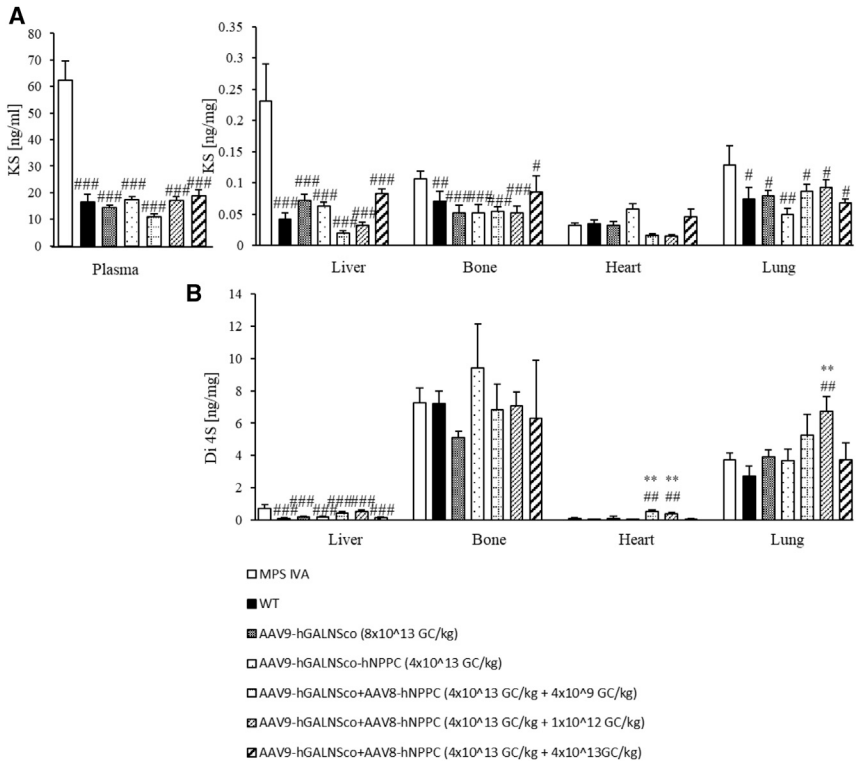

Figure 5. GAG levels in MPS IVA mice treated with AAV vectors

Seven experimental groups are presented: (1) untreated MPS IVA; (2) WT control (WT); (3) MPS IVA mice AAV9 vector expressing human GALNS enzyme (AAV9-hGALNS); (4) MPS IVA mice AAV9 vector expressing two transgenes—human GALNS enzyme and human CNP (AAV9-hGALNSco-hNPPC); and three groups (5, 6, and 7) of combination therapy with the same vectors with different dosages (AAV9-hGALNS+ AAV8-hNPPC). At 12 weeks after treatment, the level of GAG was measured: Mono-sulfated KS levels (A) plasma, liver, bone, heart, and lung; chondroitin disaccharide (Di 4S) levels in (B) liver, bone, heart, and lung. Results are shown as mean values ± SEM (n = 5). The following statistical symbols were used to denote the following vs. WT group, ***p ≤ 0.001, **p ≤ 0.01, *p ≤ 0.05; vs. untreated MPS IVA group, ###p ≤ 0.001, ##p ≤ 0.01, #p ≤ 0.05. See also Figure S2.

However, HSCT still has a minor effect on bone-related issues, although we need to increase the number of patients who undergo HSCT at an earlier stage (<2 years of age).[55] Despite these benefits, HSCT has various drawbacks, including finding a suitable donor, the risk of graft-versus-host disease, and procedure-related complications.

None of the currently available treatment options for MPS IVA patients improve bone growth. CNP maintains cartilage homeostasis and facilitates endochondral bone formation. In a mouse model, when the NPPC gene responsible for CNP production was inactivated, bone growth, birth rate, and skull size were decreased. However, no significant differences were observed in other organs or body weight.[56–59] Inducing bone growth through CNP involves binding to the Npr3 receptor located on the cell surface, followed by the downstream activation of cyclic GMP-dependent protein kinase II (discussed in Rintz et al.[60]). In our earlier experiments, we examined the effectiveness of incorporating the CNP into the AAV8 vector expression cassette for the first time. When MPS IVA mice were treated with this CNP-containing AAV vector, we observed a notable increase in growth, accompanied by consistent maintenance of body weight,[33] similar to other studies.[61–64] Furthermore, we observed a more organized chondrocyte structure within the growth plate, characterized by enhanced proliferation and differentiation.[33]

In this study, combining two distinct vectors in MPS IVA mice revealed different responses while yielding positive outcomes. Analysis of combination therapy revealed how two distinct vectors can express separate transgenes that work synergistically. The mechanism of AAV transduction in the cell starts with binding to the cell surface receptors (1), then vector encapsulated by the endosome (2), then escaping (3), entering the nucleus after uncoating the viral ssDNA (4), transcription with the use of host polymerases (5), and transgene released to the cytoplasm and going through translation (6).[65] The GALNS enzyme will go through further processing in the Golgi apparatus to be an active form of the enzyme that can act both locally and be secreted outside the cell.[19] As for CNP, after translation, it is further cleaved by cytoplasmatic enzymes to an active form of the peptide.[66,67]

The treatment approach resulted in the sustained elevation of GALNS activity in the bloodstream and notable GALNS activity in crucial target tissues, such as bone, heart, and liver. Furthermore, there was a significant decrease in the accumulation of KS both in the blood and tissues, leading to improvements in bone pathology and the promotion of bone growth in a dose-dependent manner. The experiment involved injecting two separate vectors, each expressing a different transgene or a single vector expressing both transgenes (CNP and GALNS). Initially, an equal dose of AAV expressing human *GALNS* and AAV expressing human *NPPC* (group 7) was administered. The high dose of both transgenes increased GALNS enzyme and CNP expression. However, the experiment had to be terminated at 13 weeks of age due to the overexpression of the CNP, which led to excessive growth in the mice (Figure 2). Consequently, the mice faced difficulties in movement, indicating that CNP effects are dose dependent. Thus, we decreased the dose of the CNP-expressing vector, decreasing the mouse growth to a minimum (group 6). With the middle dose of the CNP, the growth was linear without a negative outcome (group 5). We also evaluated the effect of the growth pattern in the mice after

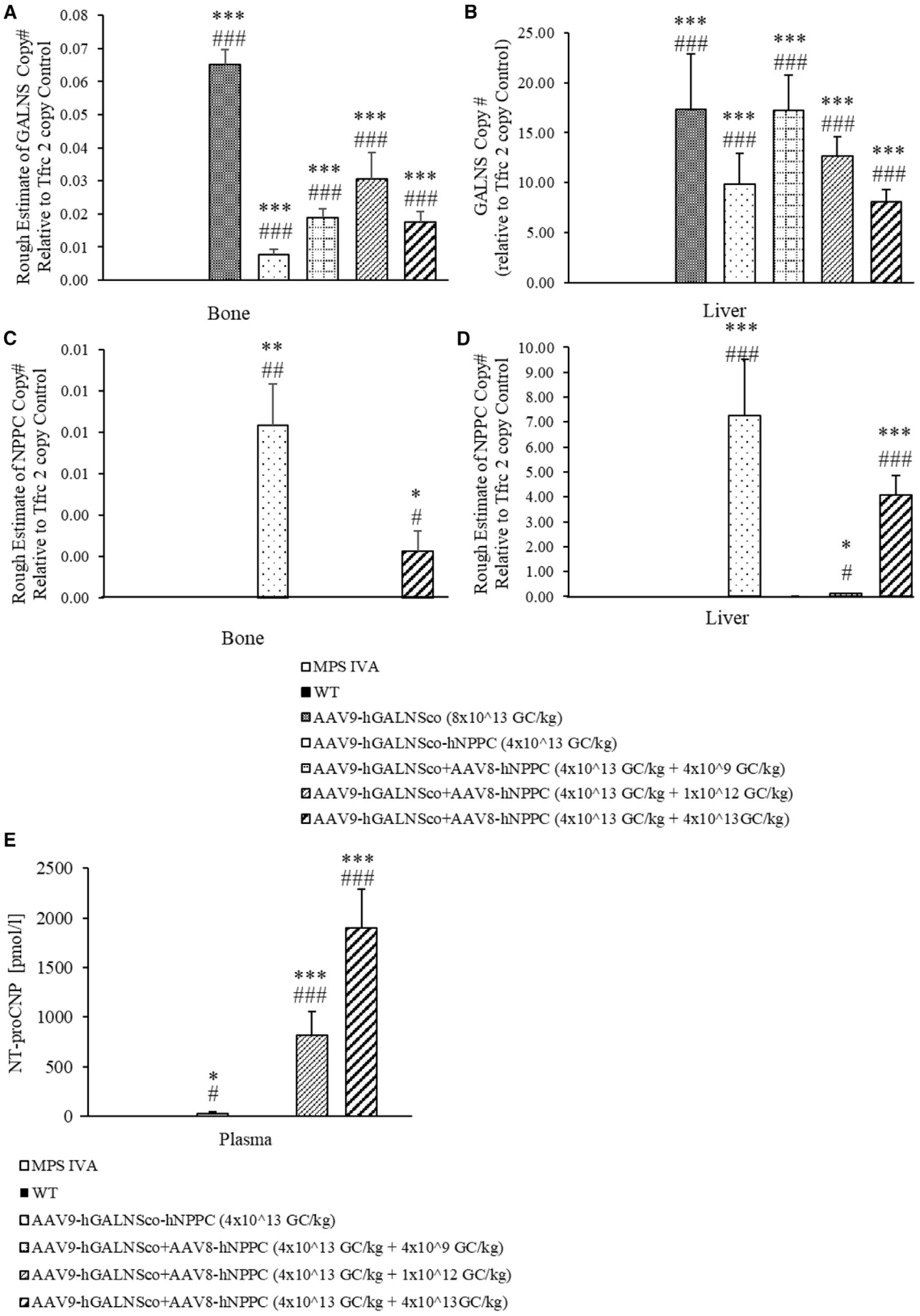

(legend on next page)

injecting one vector with two transgenes (group 4) separated with a P2A sequence. The P2A sequence enables the co-expression of multiple proteins from a single mRNA transcript by inducing ribosomal skipping during translation.[68] The growth was linear without overgrowth in this group (Figure 2). In conclusion, the bone growth seen in our study is not due to GALNS, but rather CNP. It is also critical to have the optimal CNP vector dose to avoid excessive growth. Decreasing the accumulated KS in the bone and tissues is one of the primary goals in the MPS IVA patient treatment. The KS level corresponds with the disease's clinical severity.[54,69] In humans, ERT does not change blood KS levels and skeletal symptoms[70] while improving urine KS accumulation.[71,72] Thus, circulating KS in the bloodstream might indicate better therapeutic efficacy for the skeletal symptoms.[69,73] We evaluated the efficacy of the GALNS-expressing AAV gene therapy. After administration of the AAV-containing GALNS cDNA, the enzyme activity increased in most groups 2 weeks after injection into untreated MPS IVA mice. We did not detect enzyme activity in mice treated with AAV9-hGALNS-hNPPC (group 4) (Figure 3B). In other groups, GALNS enzyme activity in plasma correlated with plasma KS level reduction at the final week of treatment. In group 4, no GALNS activity was detected. However, we observed the same decrease in the KS level as in other groups (Figure 5A). The tissue enzyme activity showed that combination therapy (groups 5–7) with two separate vectors had higher activity than one vector containing two transgenes (group 4) (Figure 3A). The greatest amount of enzyme expression was seen in the liver, but we also detected overexpression in bone, heart, and other tissues. Overexpression in the tissues correlated with the decrease in the KS level. In group 4, we did not detect the enzyme activity in bone, although GALNS activity reached the WT level in liver and heart. This might be due to the P2A sequence being too close to the *GALNS* sequence, leading to a change in the protein conformation P2A peptides lead to relatively high levels of downstream protein expression compared with other strategies for multigene co-expression, and they are small in size, thus bearing a lower risk of interfering with the function of co-expressed genes. Several different groups have successfully employed P2A peptides for polycistronic and bi-cistronic multigene expression.[74–80] Therefore, it is possible to have a high level of CNP downstream, although it impacts GALNS gene upstream because of the instability of the GALNS protein with the additional amino acid at the C-terminal. In the final week, we also detected high anti-GALNS activity in group 4, which may neutralize the GALNS activity (Figure 4B). Additionally, the GALNS protein level in liver was lower than in the other combination groups (Figure 4A). In group 4, the level of transgene expression in tissues and blood effectively decreased KS accumulation in tissues and plasma, including bones, despite there being no GALNS enzyme activity.

The biodistribution of the vectors showed that the vector expressing *GALNS* was present in both bone and liver for all tested groups (Figures 6A and 6B). In group 4, which was treated with a single vector containing two transgenes, we detected the GALNS protein in both bone and liver, although we did not detect GALNS activity in bone despite a decreased KS level in bone. A small residual activity of GALNS or cross-correction may account for this decrease. For the NPPC biodistribution, we detected it (Figures 6C and 6D) in groups 4, 6, and 7, which exhibit growth induction (Figure 2). Furthermore, we assessed the expression of human NT-proCNP as a reliable indicator of CNP expression (Figure 6E). Its extended lifespan demonstrated a noteworthy correlation with the biologically active CNP concentration, making it a valuable marker for evaluating CNP expression levels.[81] We saw a correlation between increased NT-proCNP and growth induction after treatment. Improvement of bone pathology with two vectors of a high dose of AAV8-hNPPC and AAV9-hGALNS was observed. CNP also increased the size and the number of chondrocytes in the articular cartilage and growth plate; in addition, the vacuoles decreased. It remains unknown why the high-dose group impacts the vacuolization in chondrocytes.

The bone-targeted therapy was evaluated by measuring GALNS protein expression in bone. Our findings demonstrated that a small fraction of GALNS can be provided in bone through cross-correction and direct bone targeting, as depicted in the vector biodistribution (Figure 6). Significant GALNS expression was observed primarily in bone marrow (Figure S3), with the highest levels detected in the group receiving a combination of two vectors (groups 5–7). As for the AAV9-hGALNS-injected group, the GALNS detection level was similar to the WT level (Figure S3C). Conversely, in the group receiving only one vector (group 4), GALNS staining was not detected (Figure S3D). Regarding bone pathology, micro-CT assessment did not reveal significant differences in most parameters among the various groups (Figure 7). The lack of significant differences can be attributed to challenges in mouse imaging studies, including small bone size, critical voxel size choices, potential site heterogeneity, and age-related bone loss, making subtle variations harder to detect. However, the group receiving the highest dose of the NPPC-expressing vector in combination (group 7) exhibited the most noticeable changes, which correlated with the visible alterations in the skeleton (Figure 2A). We performed bone staining with toluidine blue to

Figure 6. AAV vector biodistribution and NT-proCNP expression

Seven experimental groups are presented: (1) untreated MPS IVA; (2) WT control (WT); (3) MPS IVA mice AAV9 vector expressing human GALNS enzyme (AAV9-hGALNS); (4) MPS IVA mice AAV9 vector expressing two transgenes-human GALNS enzyme and human CNP (AAV9-hGALNSco-hNPPC); and three groups (5, 6, and 7) of combination therapy with the same vectors with different dosages (AAV9-hGALNS+ AAV8-hNPPC). Bone (A) and liver (B) GALNS vector copy number at 12 weeks after treatment; bone (C) and liver (D) NPPC vector copy number at 12 weeks after treatment. Marker for CNP expression in plasma (NT-proCNP) is higher in groups 4, 6, and 7 compared with WT and untreated MPS IVA groups (E). Results are shown as mean values ± SEM (n = 5). The following statistical symbols were used to denote comparison with ***p ≤ 0.001, **p ≤ 0.01, *p ≤ 0.05 significant differences compared with the WT group; ###p ≤ 0.001, ##p ≤ 0.01, #p ≤ 0.05 significant differences compared with the untreated MPS IVA group.

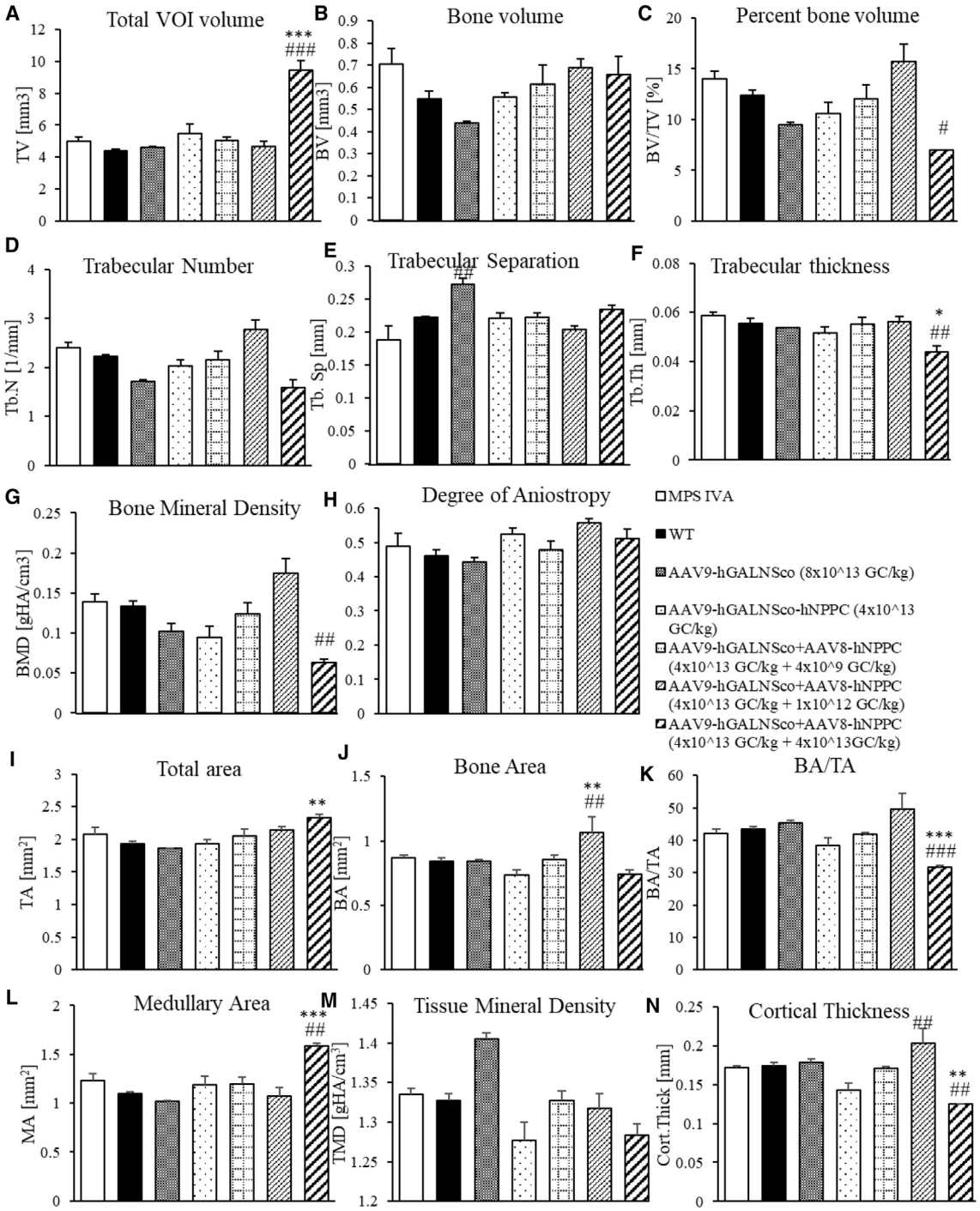

Figure 7. Trabecular and cortical morphometry after AAV vector treatment

Seven experimental groups are presented: (1) untreated MPS IVA; (2) WT control (WT); (3) MPS IVA mice AAV9 vector expressing human GALNS enzyme (AAV9-hGALNS); (4) MPS IVA mice AAV9 vector expressing two transgenes-human GALNS enzyme and human CNP (AAV9-hGALNSco-hNPPC); and three groups (5, 6, and 7) of combination therapy with the same vectors with different dosages (AAV9-hGALNS+ AAV8-hNPPC). At 12 weeks after treatment, micro-CT analysis of trabecular (A–H) and cortical (I–N) bone of seven experimental groups was performed. Trabecular analysis included (n = 5; except group 7 that was n = 3): total trabecular volume of interest (A); trabecular bone

(legend continued on next page)

evaluate the effectiveness of AAV treatment. Bone pathology revealed significant differences in the score calculation of chondrocytes (Table 1). The untreated MPS IVA chondrocytes are vacuolated with a disorganized structure (Figures 8 and S4–S6). After combination therapy of the AAV vector with CNP, we saw improvements in growth plate organization and decreased vascularization of treated chondrocytes. Our study has offered valuable insights into the potential therapeutic use of CNP for progressive skeletal dysplasia in MPS IVA. However, we must acknowledge certain limitations. First, the small sample size used in our study may affect the statistical power and the significance of the conclusions. Thus, more extensive studies are necessary to validate the effectiveness of CNP delivered through an AAV vector expression cassette in combination with the GALNS enzyme as a potential combination therapy.

Patients with MPS IVA cannot catabolize two molecules—chondroitin sulfate and KS—due to a lack of GALNS enzyme activity. As these two molecules are the main GAGs in the cartilage, their excessive accumulation in MPS IVA patients damaged cartilage tissues, including growth plates, leading to various skeletal symptoms. The growth plate region of the bone is an avascular structure, and ERT is not an accessible option for patients.[22] Earlier investigations involving the combined administration of CNP and ERT in a MPS VII mouse model demonstrated favorable results for treatment, surpassing the outcomes of individual monotherapies. This combined approach enhanced bone growth and increased enzyme activity.[82] Nonetheless, the constraints associated with ERT remain a challenge. Consequently, we propose a potentially superior long-term solution: an AAV therapy to facilitate continuous enzyme expression.

In conclusion, bone growth with high GALNS enzyme activity is proven with co-expression of GALNS and CNP genes, especially in separate cassette vectors. It is recommended that the optimal dose of the CNP vector is defined with a more significant number of mice to eliminate undesired overgrowth and adverse effects, moving forward to a clinical trial. It may be considered to add a microRNA system[83,84] to stop the CNP gene expression when we observe the excessive growth.

MATERIALS AND METHODS

Expression vector

To overexpress the human native NPPC gene and/or codon-optimized human GALNS enzyme gene, three AAV vectors were used: pAAV[Exp]-CAG>hNPPC[NM_024409.4]:WPRE; pAAV[Exp]-CAG>{hGALNSco}:WPRE; pAAV[Exp]-CAG>hGALNS[NM_001323544.2](ns):P2A:hNPPC[NM_024409.4]:WPRE (VectorBuilder, Chicago, IL, USA).

Experimental design

All procedures for this study were approved by the Institutional Animal Care and Use Committee of Nemours Children's Health. Mice were housed in a 12/12h light/dark cycle with food and water provided *ad libitum*. The experimental design is shown in Figure 1B, with seven experimental groups (n = 5, unless stated otherwise), two control groups (WT and untreated MPS IVA), and five treated groups (groups 3–7). We injected 4-week-old male mice intravenously with one or two of the AAV vector(s) (Figure 1A) depending on the experimental group, as shown in Figure 1B. In the case of groups 3 and 4, mice were injected with one vector. As for groups 5–7, mice were injected with two vectors; the AAV9-hGALNS vector was injected with the same dose of 4×10^{13} GC/kg, while the dosage of the AAV8-hNPPC differs in the groups (group 5: 4×10^{9} GC/kg; group 6: 1×10^{12} GC/kg; and group 5: 4×10^{13} GC/kg). Mice were measured (length and weight) weekly, and blood was collected biweekly for 12 constitutive weeks. At 16 weeks of age, mice were euthanized in a CO_2 chamber and perfused with 10 mL 0.9% saline, except for group 7, which was euthanized at 13 weeks. Tissues were collected for further analysis.

MPS IVA mouse model

This study used a previously described mouse model of the MPS IVA knockout mice (MKC2; C57BL/6 background).[33] Mice did not have GALNS enzyme activity and showed an accumulation of storage material in many tissues and plasma. We performed genotyping at 20 days of age by PCR. Primers were designed to flank each single guide RNA site, allowing for the evaluation of individual nonhomologous DNA end-joining activity and screening for deletion mutations between the two target sites when paired.

Cell lines

Human fibroblasts (either a healthy patient or MPS IVA patient) were plated onto six-well plates (3×10^{5} cells/well) and incubated overnight at 37°C in a humidified 5% CO_2 incubator before transduction. After incubation, cells were transduced with the AAV9-hGALNS vector at MOI 10^{5}/well and 10^{6}/well. The next day, we changed the medium of the cells. At 48 h after transduction, we collected cells for GALNS enzyme assay measurement.

GALNS enzyme activity assay

A GALNS enzyme activity assay was performed as previously described.[33] Human fibroblast pellets were lysed with the lysis buffer (25 mM/L Tris-HCl (pH 7.2) and 1 mM/L phenylmethylsulphonyl fluoride). Then, lysed cells were centrifuged for 30 min at 4°C, and the supernatant was collected in a new tube and assayed for enzyme activity. Tissues were homogenized with Bead Mill Homogenizer (OMNI International, Kennesaw, GA, USA) supernatant was used

volume (B), percent bone volume (C), trabecular number (D), trabecular separation (E), trabecular thickness (F), bone mineral density (G), and degree of anisotropy (H). Cortical analysis included (n = 5; except group 7, n = 3): Total area (I), cortical bone area (J), bone area/total area (K), medullary area (L), tissue mineral density (M), and cortical thickness (N). Results are shown as mean values ± SEM. The following statistical symbols were used to denote comparison with ***p ≤ 0.001, **p ≤ 0.01, *p ≤ 0.05 significant differences compared with the WT group; ###p ≤ 0.001, ##p ≤ 0.01, #p ≤ 0.05 significant differences compared with the untreated MPS IVA group.

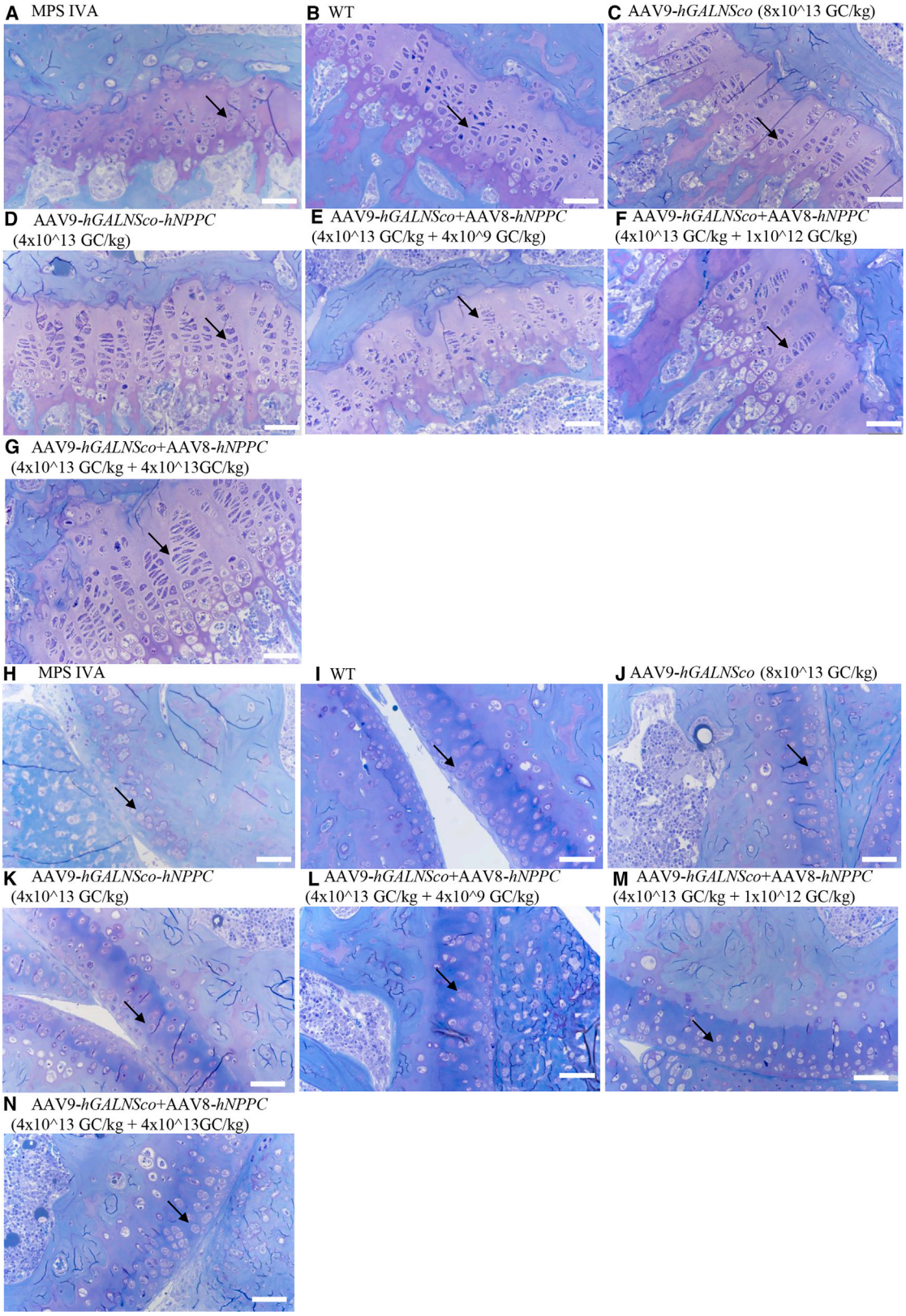

(legend on next page)

for the assay. Either tissue/cell lysate or plasma (2 μL) was used for the enzymatic reaction with 22 mM 4-methylumbelliferyl-β-galactopyranoside-6-sulfate (Research Products International, Mount Prospect, IL, USA) and incubated at 37°C for 16 h. After incubation, 10 mg/mL β-galactosidase from *Aspergillus oryzae* (Sigma-Aldrich, St. Louis, MO, USA) was added and incubated for 2 h at 37°C. To stop the reaction, a 1 M glycine NaOH solution (pH 10.5) was used, and the resulting mixture was subjected to measurement using a FLUOstar Omega plate reader (BMG LABTECH Inc., Cary, NC, USA) at an excitation wavelength of 366 nm and an emission wavelength of 450 nm. The enzyme activity is expressed as nanomoles of 4-methylumbelliferone released per hour per microliter of plasma or milligram of protein. The protein concentration in the samples was determined using a bicinchoninic acid protein assay kit (Thermo Fisher Scientific, Waltham, MA, USA).

GAGs quantification

GAG assay was determined in plasma and tissues as previously described.[32]

Bone pathological assessments

Tissue staining and analysis were performed as described previously.[32,33] Briefly, knee joints were collected from 16-week-old MPS IVA and WT mice to evaluate levels of storage granules by light microscopy. Tissues were fixed in 2% paraformaldehyde and 4% glutaraldehyde in PBS, post-fixed in osmium tetroxide, and embedded in Spurr's resin. Then, toluidine blue-stained 0.5-μm-thick sections were examined. To evaluate chondrocyte cell size (vacuolization) in the growth plates of femur or tibia, approximately 300 chondrocytes in the proliferative area were measured in each mouse by ImageJ software, and results were expressed as folds-change from the WT group. Pathological slides from knee joints of treated and untreated MPS IVA and WT mice were evaluated for reduced vacuolization and improved column orientation in growth plates (Table 1). The amount of storage materials and the degree of disoriented columns were scored. No storage or very slight was 0 (−), slight but obvious was 1 (+), moderate was 2 (++), and marked was 3 (+++). Each pathological slide was assessed in a double-blind manner three times.[33] We then averaged the scores in a group of mice per section of bone (growth plate, articular disc, meniscus, and ligament).

Trabecular and cortical morphometry

Trabecular and cortical morphometry measurements were carried out using micro-CT scans performed with a Bruker SkyScan 1275 scanner (Bruker, Billerica, MA, USA) as previously described.[33] To prepare the samples, the right femur from 16-week-old mice was fixed using 96% ethanol. Prior to analysis, the femur was carefully wrapped in gauze soaked in 0.9% NaCl and subjected to scanning. Quantitative analysis was conducted using Bruker CTan software (v1.21.1.0). The regions of interest (ROIs) for trabecular bone were identified by focusing on the distal epiphyseal plate. As for cortical bone, the ROIs were determined based on the starting point of the distal epiphyseal plate and the highest point in the proximal greater trochanter. The total length of the bone was obtained by considering the area between these two landmarks.

AAV vector genome biodistribution

dPCR was performed to assess the biodistribution of DNA vectors. For this purpose, DNA was extracted from the liver with the Gentra Puregene kit, following the manufacturer's instructions (-QIAGEN, Germantown, MD, USA). As for the bone, prior to purification, it was homogenized using the Bead Mill Homogenizer (OMNI International), and subsequently purified according to the provided guidelines (QIAGEN). To perform dPCR analysis, specific primers and probe sequences targeting either the NPPC or GALNS gene (Table S2) were used to amplify genomic DNA obtained from liver and bone samples of mice. Genomic DNA was tested in both non-fragmented and fragmented forms, the latter achieved through enzymatic digestion or an M220 Focused-ultrasonicator (Covaris, Woburn, MA, USA). Quantitative dPCR analysis of the AAV CNP-expressing vector was conducted using the TaqMan assay (FAM-labeled) (Thermo Fisher Scientific, Waltham, MA, USA). The DNA concentration for the AAV chip in the liver and bone samples ranged between 0.5 and 2 ng per 16-mL reaction, depending on the required DNA concentration to ensure detectability on the instrument. The Tfrc TaqMan copy number reference assay (VIC labeled) was acquired from Thermo Fisher Scientific. For the Tfrc dPCR, 40 ng genomic DNA per 16-mL reaction was utilized. Each reaction was loaded onto a separate QuantStudio chip (QuantStudio 3D digital PCR 20K chip kit v2, A26316; Thermo Fisher Scientific). PCR amplification was carried out using an ABI GeneAmp 9700 PCR thermal cycler with dual flat blocks (Applied Biosystems, Waltham, MA, USA). The QuantStudio 3D instrument was employed to read the chips, enabling the determination of the number of wells positive for the VIC and FAM channels, as well as the number of wells without DNA and empty wells. Subsequent data analysis and chip quality assessment were performed using the QuantStudio 3D

Figure 8. Correction of bone pathology in MPS IVA mice treated with AAV vectors assessed by toluidine blue staining analysis using light microscopy

Seven experimental groups are presented: (1) untreated MPS IVA; (2) WT control (WT); (3) MPS IVA mice AAV9 vector expressing human GALNS enzyme (AAV9-hGALNS); (4) MPS IVA mice AAV9 vector expressing two transgenes-human GALNS enzyme and human CNP (AAV9-hGALNSco-hNPPC); and three groups (5, 6, and 7) of combination therapy with the same vectors with different dosages (AAV9-hGALNS+ AAV8-hNPPC). Tibia growth plate of untreated MPS IVA (A), WT (B), AAV9-hGALNSco (8×10^{13} GC/kg) (C), AAV9-hGALNSco-hNPPC (4×10^{13} GC/kg) (D), AAV9-hGALNSco+AAV8-hNPPC (4×10^{13} GC/kg + 4×10^{9} GC/kg) (E), AAV9-hGALNSco+AAV8-hNPPC (4×10^{13} GC/kg + 1×10^{12} GC/kg) (F), and AAV9-hGALNSco+AAV8-hNPPC (4×10^{13} GC/kg + 4×10^{13} GC/kg) (G). Tibia articular cartilage of untreated MPS IVA (H), WT (I), AAV9-hGALNSco (8×10^{13} GC/kg) (J), AAV9-hGALNSco-hNPPC (4×10^{13} GC/kg) (K), AAV9-hGALNSco + AAV8-hNPPC (4×10^{13} GC/kg + 4×10^{9} GC/kg) (L), AAV9-hGALNSco + AAV8-hNPPC (4×10^{13} GC/kg + 1×10^{12} GC/kg) (M), and AAV9-hGALNSco+AAV8-hNPPC (4×10^{13} GC/kg + 4×10^{13} GC/kg) (N). Original magnification ×40, with 500-μm scale bar. Arrows show chondrocytes. See also Figures S4–S6.

Table 1. Pathological scores in bone of MPS IVA mice treated with AAV vectors

Bone	Structure	Finding	MPS IVA –	WT –	AAV9-hGALNSco 8×10^{13} GC/kg	AAV9-hGALNSco-hNPPC 4×10^{13} GC/kg	AAV9-hGALNSco+ AAV8-hNPPC 4×10^{13} GC/kg $+4 \times 10^{9}$ GC/kg	AAV9-hGALNSco+ AAV8-hNPPC 4×10^{13} GC/kg $+1 \times 10^{12}$ GC/kg	AAV9-hGALNSco+ AAV8-hNPPC 4×10^{13} GC/kg $+4 \times 10^{13}$ GC/kg
Tibia	growth plate	vacuolization	2.9 ± 0.1	0.0	2.8 ± 0.1	2.9 ± 0.1	2.9 ± 0.1	2.4 ± 0.2	2.4 ± 0.3 #
		column structure	2.8 ± 0.1	0.0	2.5 ± 0.1	2.6 ± 0.2	2.7 ± 0.1	2.1 ± 0.2 #	2.2 ± 0.2 #
	articular cartilage	vacuolization	2.9 ± 0.1	0.0	2.8 ± 0.1	2.9 ± 0.1	2.7 ± 0.1 #	2.7 ± 0.1 #	2.6 ± 0.1 #
		column structure	2.9 ± 0.2	0.0	2.7 ± 0.1 #	2.8 ± 0.1	2.7 ± 0.1 #	2.5 ± 0.1 #	2.4 ± 0.1 #
Femur	growth plate	vacuolization	2.8 ± 0.2	0.0	2.9 ± 0.1	3.0 ± 0.1	3.0 ± 0.1	2.7 ± 0.1	2.2 ± 0.1 #
		column structure	3.0 ± 0.1	0.0	2.8 ± 0.1	2.8 ± 0.1	3.0 ± 0.1	2.5 ± 0.1 #	2.1 ± 0.3 #
	articular cartilage	vacuolization	2.9 ± 0.1	0.0	2.8 ± 0.1	2.8 ± 0.1	2.8 ± 0.1	2.6 ± 0.1 #	2.3 ± 0.2 #
		column structure	2.9 ± 0.1	0.0	2.6 ± 0.1	2.8 ± 0.1	2.8 ± 0.1	2.5 ± 0.1	2.2 ± 0.1 #
Ligament		vacuolization	3.0 ± 0.0	0.0	N/A	3.0 ± 0.0	2.7 ± 0.2	2.3 ± 0.1 #	2.0 ± 0.1 #
Meniscus		vacuolization	2.9 ± 0.1	0.0	2.7 ± 0.2	3.0 ± 0.0	2.7 ± 0.2	2.7 ± 0.1	2.6 ± 0.2

Results are shown as mean values ± SEM (n = 4–7). The following statistical symbols were used to denote comparison with #$p \leq 0.01$, significant differences to untreated MPS IVA group.
N/A, not available.

analysis suite. All chips contained between 25% and 75% empty wells, ensuring their suitability for quantitation. Copies per milliliter for both Tfrc and AAV were calculated and normalized using the dilution factor for the AAV sample input. The number of AAV copies per mouse genome was calculated by employing the Tfrc results as a reference for two copies.

ELISA

NT-proCNP was detected in mice according to manufacturer instructions (Biomedica Medizinprodukte, Vienna, Austria). Sample preparation included blood collected from mice to be centrifuged at 8,000×*g* at 4°C for 10 min to collect plasma sample to another tube and stored at −20°C until further analysis. Plasma used for NT-proCNP detection was diluted 1:100 in the assay buffer provided in the ELISA kit.

Anti-GALNS IgG and IgE antibodies was detected by indirect ELISA in treated and untreated mice according to a previously published paper.[85] Ninety-six-well polystyrene microplates were coated with 2 μg/L rh galactosamine (N-acetyl)-6-sulfatase/GALNS; lot#DDJU0319021 (R&D Systems, Minneapolis, MN, USA) (0.2 μg/well) diluted in coating buffer (15 mM Na_2CO_3 , 35 mM $NaHCO_3$, 0.02% NaN_3, pH = 9.6) and incubated overnight at 4°C. After overnight incubation, the plate was washed with TBST buffer (TBS-Tween: 10 mM Tris pH = 7.5, 150 mM NaCl, 0.05% Tween 20). The plate was blocked for 1 h with 3% bovine serum. Plasma (1:100 dilution in TBST) or standard (GALNS Polyclonal rabbit antibodies cat#PA5-22098; 1 mg/mL; 100 μL) was added and incubated for 2.5 h at 37°C. After incubation, the plate was washed 4× with TBST, and then 100 μL peroxidase substrate TMB (3,3′,5,5′-tetramethylbenzidine; Thermo Fisher Scientific) was added and incubated for 30 min at RT on moving rotor. The reaction was stopped with 1N HCl. The plate was read at 450 nm, and the OD was measured using a FLUOstar Omega plate reader (BMG LABTECH Inc.).

Immunohistology staining

Tibia was collected in the final week and fixed in 10% formalin. Formalin-fixed paraffin-embedded samples were processed from fixed tissue. The samples were cut at 5 μm on a Leica RM2255 microtome (Leica, Buffalo Grove, IL, USA) and floated onto Superfrost Plus slides (Thermo Fisher Scientific, Fremont, CA, USA). The sections were heat immobilized for 60 min in a 60°C oven. Slides were deparaffinized on a Sakura (Torrance, CA, USA) Stainer using xylene, 100% ETOH, 95% ETOH, and 80% ETOH. Antigen retrieval was performed by adding slides to Bond ER 2 solution (Leica) in a 60°C oven overnight, cooled down, and then rinsed in de-ionized water, after which the slides were stained using the Novolink Min Polymer Detection System (Leica Biosystems-RE7290-K). The slides were rinsed in Bond Wash (Leica-AR-9590), and then briefly placed into peroxidase block, rinsed in bond wash, then incubated in their prospective antibody: rabbit anti-GALNS (Creative Biolabs, Shirley, NY, USA) for 30 min. The slides were then rinsed in bond wash solution and incubated in the polymer. After additional rinses of bond wash, the slides were developed in the DAB kit, rinsed, and then counterstained with hematoxylin from the kit. The slides were rinsed in de-ionized water and then placed on the Sakura Tissue-Tek Prisma Automated Stainer/Coverslipper (Sakura, Torrance, CA, USA), dehydrated, cleared, and then mounted in Tissue Tek Glas mounting media (Sakura). The area of CNP expression was calculated with ImageJ software.

Western blot

Protein lysate was isolated from both the liver and arm bone, as described in the "GALNS enzyme activity assay" section. After lysis

and determination of protein concentration, the protein extracts were separated by electrophoresis. However, we did not obtain a sufficient protein concentration in the bone tissue for further analysis. Therefore, only the liver tissue was analyzed for protein expression. After electrophoresis, the proteins were transferred onto a nitrocellulose membrane. The membrane was blocked with 5% nonfat dry milk in TBST buffer and then incubated with primary antibodies overnight at 4°C (rabbit anti-GALNS [Creative Biolabs] and beta-actin [Sigma-Aldrich, St. Louis, MO, USA]). The membrane was subsequently incubated with secondary antibodies at room temperature for 1 h, treated with a solution of substrates for horserasish peroxidase detection, and read with a C-DiGiT Blot Scanner Licor Machine. As CNP and beta-actin have similar protein weights, the membrane was stripped after performing analysis for the CNP protein, and beta-actin analysis was performed starting from the blocking step. The intensities of bands were analyzed using the QuantityOne software.

Statistical analysis

The normal distribution was found using the Kolmogorov-Smirnov test and homogeneity of variance with the Leven test. Depending on the results, analysis of variance (two-way ANOVA) with Tukey's *post hoc* test was performed if the distribution was normal. When the assumptions of the normality of the distribution and the homogeneity of variance were unmet, the nonparametric Kruskall-Wallis test, followed by Dunnett's test, was performed. Statistical analyses were performed using GraphPad Prism 9 software. Statistical significance was set at a p value of >0.05. Error bars represent SEM, as indicated in legends.

DATA AND CODE AVAILABILITY

The data that support the findings of this study are available on request from the corresponding author (S.T.).

SUPPLEMENTAL INFORMATION

Supplemental information can be found online at https://doi.org/10.1016/j.omtn.2024.102211.

ACKNOWLEDGMENTS

This work was also supported by grants from the Austrian MPS society, A Cure for Robert, Inc., The Carol Ann Foundation, Angelo R. Cali & Mary V. Cali Family Foundation, Inc., The Vain and Harry Fish Foundation, Inc., The Bennett Foundation, Jacob Randall Foundation, and Nemours Funds. S.T. was supported by an Institutional Development Award from the Eunice Kennedy Shriver National Institute of Child Health & Human Development of the National Institutes of Health (NICHD) (1R01HD102545-01A1).

AUTHOR CONTRIBUTIONS

Conceptualization, E.R., S.T.; methodology, E.R., S.K., and F.N.; validation, E.R.; formal analysis, E.R.; investigation, E.R.; resources, S.T.; data curation, E.R., A.M.H.-P., B.C., S.K., F.N., and E.B.-F.; writing—original draft preparation, E.R.; writing—review and editing, S.T.; visualization, E.R.; supervision, S.T.; project administration, S.T.; funding acquisition, S.T. All authors have read and agreed to the published version of the manuscript.

DECLARATION OF INTERESTS

The authors declare no conflict of interest.

REFERENCES

1. Çelik, B., Tomatsu, S.C., Tomatsu, S., and Khan, S.A. (2021). Epidemiology of Mucopolysaccharidoses Update. Diagnostics *11*, 273. https://doi.org/10.3390/diagnostics11020273.

2. Kubaski, F., de Oliveira Poswar, F., Michelin-Tirelli, K., Burin, M.G., Rojas-Málaga, D., Brusius-Facchin, A.C., Leistner-Segal, S., and Giugliani, R. (2020). Diagnosis of Mucopolysaccharidoses. Diagnostics *10*, 172. https://doi.org/10.3390/diagnostics10030172.

3. Giugliani, R. (2012). Mucopolysacccharidoses: From understanding to treatment., a century of discoveries. Genet. Mol. Biol. *35*, 924–931. https://doi.org/10.1590/s1415-47572012000600006.

4. Verheyen, S., Blatterer, J., Speicher, M.R., Bhavani, G.S., Boons, G.J., Ilse, M.B., Andrae, D., Sproß, J., Vaz, F.M., Kircher, S.G., et al. (2022). Novel subtype of mucopolysaccharidosis caused by arylsulfatase K (ARSK) deficiency. J. Med. Genet. *59*, 957–964. https://doi.org/10.1136/jmedgenet-2021-108061.

5. Nagpal, R., Goyal, R.B., Priyadarshini, K., Kashyap, S., Sharma, M., Sinha, R., and Sharma, N. (2022). Mucopolysaccharidosis: A broad review. Indian J. Ophthalmol. *70*, 2249–2261. https://doi.org/10.4103/ijo.IJO_425_22.

6. Rintz, E., Pierzynowska, K., Podlacha, M., and Węgrzyn, G. (2020). Has resveratrol a potential for mucopolysaccharidosis treatment? Eur. J. Pharmacol. *888*, 173534. https://doi.org/10.1016/j.ejphar.2020.173534.

7. Nan, H., Park, C., and Maeng, S. (2020). Mucopolysaccharidoses I and II: Brief Review of Therapeutic Options and Supportive/Palliative Therapies. BioMed Res. Int. *2020*, 2408402. https://doi.org/10.1155/2020/2408402.

8. Stapleton, M., Arunkumar, N., Kubaski, F., Mason, R.W., Tadao, O., and Tomatsu, S. (2018). Clinical presentation and diagnosis of mucopolysaccharidoses. Mol. Genet. Metabol. *125*, 4–17. https://doi.org/10.1016/j.ymgme.2018.01.003.

9. Zhang, W., Liu, Q.Y., Haqqani, A.S., Leclerc, S., Liu, Z., Fauteux, F., Baumann, E., Delaney, C.E., Ly, D., Star, A.T., et al. (2020). Differential expression of receptors mediating receptor-mediated transcytosis (RMT) in brain microvessels., brain parenchyma and peripheral tissues of the mouse and the human. Fluids Barriers CNS *17*, 47. https://doi.org/10.1186/s12987-020-00209-0.

10. Sawamoto, K., Chen, H.H., Alméciga-Díaz, C.J., Mason, R.W., and Tomatsu, S. (2018). Gene therapy for Mucopolysaccharidoses. Mol. Genet. Metabol. *123*, 59–68. https://doi.org/10.1016/j.ymgme.2017.12.434.

11. Acosta, W., Ayala, J., Dolan, M.C., and Cramer, C.L. (2015). RTB Lectin: a novel receptor-independent delivery system for lysosomal enzyme replacement therapies. Sci. Rep. *5*, 14144. https://doi.org/10.1038/srep14144.

12. Boado, R.J., Zhang, Y., Zhang, Y., Xia, C.F., Wang, Y., and Pardridge, W.M. (2008). Genetic engineering of a lysosomal enzyme fusion protein for targeted delivery across the human blood-brain barrier. Biotechnol. Bioeng. *99*, 475–484. https://doi.org/10.1002/bit.21602.

13. Kida, S., Koshimura, Y., Yoden, E., Yoshioka, A., Morimoto, H., Imakiire, A., Tanaka, N., Tanaka, S., Mori, A., Ito, J., et al. (2023). Enzyme replacement with transferrin receptor-targeted α-L-iduronidase rescues brain pathology in mucopolysaccharidosis I mice. Mol. Ther. Methods Clin. Dev. *29*, 439–449. https://doi.org/10.1016/j.omtm.2023.05.010.

14. Lu, J.Z., Hui, E.K.W., Boado, R.J., and Pardridge, W.M. (2010). Genetic engineering of a bifunctional IgG fusion protein with iduronate-2-sulfatase. Bioconjugate Chem. *21*, 151–156. https://doi.org/10.1021/bc900382q.

15. Sonoda, H., Morimoto, H., Yoden, E., Koshimura, Y., Kinoshita, M., Golovina, G., Takagi, H., Yamamoto, R., Minami, K., Mizoguchi, A., et al. (2018). A Blood-Brain-Barrier-Penetrating Anti-human Transferrin Receptor Antibody Fusion Protein for Neuronopathic Mucopolysaccharidosis II. Mol. Ther. *26*, 1366–1374. https://doi.org/10.1016/j.ymthe.2018.02.032.

16. Kan, S.H., Troitskaya, L.A., Sinow, C.S., Haitz, K., Todd, A.K., Di Stefano, A., Le, S.Q., Dickson, P.I., and Tippin, B.L. (2014). Insulin-like growth factor II peptide fusion enables uptake and lysosomal delivery of α-N-acetylglucosaminidase to mucopolysaccharidosis type IIIB fibroblasts. Biochem. J. *458*, 281–289. https://doi.org/10.1042/BJ20130845.

17. Boado, R.J., Lu, J.Z., Hui, E.K.W., Lin, H., and Pardridge, W.M. (2016). Insulin Receptor Antibody-α-N-Acetylglucosaminidase Fusion Protein Penetrates the Primate Blood-Brain Barrier and Reduces Glycosoaminoglycans in Sanfilippo Type B Fibroblasts. Mol. Pharm. *13*, 1385–1392. https://doi.org/10.1021/acs.molpharmaceut.6b00037.

18. Boado, R.J., and Pardridge, W.M. (2010). Genetic engineering of IgG-glucuronidase fusion proteins. J. Drug Target. *18*, 205–211. https://doi.org/10.3109/10611860903353362.

19. Leal, A.F., Benincore-Flórez, E., Rintz, E., Herreño-Pachón, A.M., Celik, B., Ago, Y., Alméciga-Díaz, C.J., and Tomatsu, S. (2022). Mucopolysaccharidoses: Cellular Consequences of Glycosaminoglycans Accumulation and Potential Targets. Int. J. Mol. Sci. *24*, 477. https://doi.org/10.3390/ijms24010477.

20. Hampe, C.S., Wesley, J., Lund, T.C., Orchard, P.J., Polgreen, L.E., Eisengart, J.B., McLoon, L.K., Cureoglu, S., Schachern, P., and McIvor, R.S. (2021). Mucopolysaccharidosis Type I: Current Treatments., Limitations., and Prospects for Improvement. Biomolecules *11*, 189. https://doi.org/10.3390/biom11020189.

21. Schmidt, M., Breyer, S., Löbel, U., Yarar, S., Stücker, R., Ullrich, K., Müller, I., and Muschol, N. (2016). Musculoskeletal manifestations in mucopolysaccharidosis type I (Hurler syndrome) following hematopoietic stem cell transplantation. Orphanet J. Rare Dis. *11*, 93. https://doi.org/10.1186/s13023-016-0470-7.

22. Sawamoto, K., Álvarez González, J.V., Piechnik, M., Otero, F.J., Couce, M.L., Suzuki, Y., and Tomatsu, S. (2020). Mucopolysaccharidosis IVA: Diagnosis., Treatment., and Management. Int. J. Mol. Sci. *21*, 1517. https://doi.org/10.3390/ijms21041517.

23. Gatto, F., Redaelli, D., Salvadè, A., Marzorati, S., Sacchetti, B., Ferina, C., Roobrouck, V.D., Bertola, F., Romano, M., Villani, G., et al. (2012). Hurler disease bone marrow stromal cells exhibit altered ability to support osteoclast formation. Stem Cell. Dev. *21*, 1466–1477. https://doi.org/10.1089/scd.2011.0555.

24. Fung, E.B., Johnson, J.A., Madden, J., Kim, T., and Harmatz, P. (2010). Bone density assessment in patients with mucopolysaccharidosis: A preliminary report from patients with MPS II and VI. J. Pediatr. Rehabil. Med. *3*, 13–23.

25. Nur, B.G., Nur, H., and Mihci, E. (2017). Bone mineral density in patients with mucopolysaccharidosis type III. J. Bone Miner. Metabol. *35*, 338–343. https://doi.org/10.1007/s00774-016-0762-y. E.

26. Khan, S., Alméciga-Díaz, C.J., Sawamoto, K., Mackenzie, W.G., Theroux, M.C., Pizarro, C., Mason, R.W., Orii, T., and Tomatsu, S. (2017). Mucopolysaccharidosis IVA and glycosaminoglycans. Mol. Genet. Metabol. *120*, 78–95. https://doi.org/10.1016/j.ymgme.2016.11.007.

27. Gafni, Y., Pelled, G., Zilberman, Y., Turgeman, G., Apparailly, F., Yotvat, H., Galun, E., Gazit, Z., Jorgensen, C., and Gazit, D. (2004). Gene therapy platform for bone regeneration using an exogenously regulated, AAV-2-based gene expression system. Mol. Ther. *9*, 587–595. https://doi.org/10.1016/j.ymthe.2003.12.009.

28. Dai, J., and Rabie, A.B.M. (2007). The use of recombinant adeno-associated virus for skeletal gene therapy. Orthod. Craniofac. Res. *10*, 1–14. https://doi.org/10.1111/j.1601-6343.2007.00381.x.

29. Yang, Y.S., Xie, J., Chaugule, S., Wang, D., Kim, J.M., Kim, J., Tai, P.W.L., Seo, S.K., Gravallese, E., Gao, G., and Shim, J.H. (2020). Bone-Targeting AAV-Mediated Gene Silencing in Osteoclasts for Osteoporosis Therapy. Mol. Ther. Methods Clin. Dev. *17*, 922–935. https://doi.org/10.1016/j.omtm.2020.04.010.

30. Yang, Y.S., Sato, T., Chaugule, S., Ma, H., Xie, J., Gao, G., and Shim, J.H. (2024). AAV-based gene editing of type 1 collagen mutation to treat osteogenesis imperfecta. Mol. Ther. Nucleic Acids *35*, 102111. https://doi.org/10.1016/j.omtn.2023.102111.

31. Piechnik, M., Amendum, P.C., Sawamoto, K., Stapleton, M., Khan, S., Fnu, N., Álvarez, V., Pachon, A.M.H., Danos, O., Bruder, J.T., et al. (2022). Sex Difference Leads to Differential Gene Expression Patterns and Therapeutic Efficacy in Mucopolysaccharidosis IVA Murine Model Receiving AAV8 Gene Therapy. Int. J. Mol. Sci. *23*, 12693. https://doi.org/10.3390/ijms232012693.

32. Sawamoto, K., Karumuthil-Melethil, S., Khan, S., Stapleton, M., Bruder, J.T., Danos, O., and Tomatsu, S. (2020). Liver-Targeted AAV8 Gene Therapy Ameliorates Skeletal and Cardiovascular Pathology in a Mucopolysaccharidosis IVA Murine Model. Mol. Ther. Methods Clin. Dev. *18*, 50–61. https://doi.org/10.1016/j.omtm.2020.05.015.

33. Rintz, E., Herreño-Pachón, A.M., Celik, B., Nidhi, F., Khan, S., Benincore-Flórez, E., and Tomatsu, S. (2023). Bone Growth Induction in Mucopolysaccharidosis IVA Mouse. Int. J. Mol. Sci. *24*, 9890. https://doi.org/10.3390/ijms24129890.

34. Chen, S.K., Hawley, Z.C.E., Zavodszky, M.I., Hana, S., Ferretti, D., Grubor, B., Hawes, M., Xu, S., Hamann, S., Marsh, G., et al. (2023). Efficacy and safety of a SOD1-targeting artificial miRNA delivered by AAV9 in mice are impacted by miRNA scaffold selection. Mol. Ther. Nucleic Acids *34*, 102057. https://doi.org/10.1016/j.omtn.2023.102057.

35. Vercauteren, K., Hoffman, B.E., Zolotukhin, I., Keeler, G.D., Xiao, J.W., Basner-Tschakarjan, E., High, K.A., Ertl, H.C., Rice, C.M., Srivastava, A., et al. (2016). Superior In vivo Transduction of Human Hepatocytes Using Engineered AAV3 Capsid. Mol. Ther. *24*, 1042–1049. https://doi.org/10.1038/mt.2016.61.

36. Inagaki, K., Fuess, S., Storm, T.A., Gibson, G.A., Mctiernan, C.F., Kay, M.A., and Nakai, H. (2006). Robust systemic transduction with AAV9 vectors in mice: efficient global cardiac gene transfer superior to that of AAV8. Mol. Ther. *14*, 45–53. https://doi.org/10.1016/j.ymthe.2006.03.014.

37. Issa, S.S., Shaimardanova, A.A., Solovyeva, V.V., and Rizvanov, A.A. (2023). Various AAV Serotypes and Their Applications in Gene Therapy: An Overview. Cells *12*, 785. https://doi.org/10.3390/cells12050785.

38. Su, J., She, K., Song, L., Jin, X., Li, R., Zhao, Q., Xiao, J., Chen, D., Cheng, H., Lu, F., et al. (2023). In vivo base editing rescues photoreceptors in a mouse model of retinitis pigmentosa. Mol. Ther. Nucleic Acids *31*, 596–609. https://doi.org/10.1016/j.omtn.2023.02.011.

39. Rubin, J.D., Nguyen, T.V., Allen, K.L., Ayasoufi, K., and Barry, M.A. (2019). Comparison of Gene Delivery to the Kidney by Adenovirus, Adeno-Associated Virus, and Lentiviral Vectors After Intravenous and Direct Kidney Injections. Hum. Gene Ther. *30*, 1559–1571. https://doi.org/10.1089/hum.2019.127.

40. Wang, A.Y., Peng, P.D., Ehrhardt, A., Storm, T.A., and Kay, M.A. (2004). Comparison of adenoviral and adeno-associated viral vectors for pancreatic gene delivery *in vivo*. Hum. Gene Ther. *15*, 405–413. https://doi.org/10.1089/104303404322959551.

41. Zincarelli, C., Soltys, S., Rengo, G., and Rabinowitz, J.E. (2008). Analysis of AAV serotypes 1-9 mediated gene expression and tropism in mice after systemic injection. Mol. Ther. *16*, 1073–1080. https://doi.org/10.1038/mt.2008.76.

42. Nam, H.J., Lane, M.D., Padron, E., Gurda, B., McKenna, R., Kohlbrenner, E., Aslanidi, G., Byrne, B., Muzyczka, N., Zolotukhin, S., and Agbandje-McKenna, M. (2007). Structure of adeno-associated virus serotype 8, a gene therapy vector. J. Virol. *81*, 12260–12271. https://doi.org/10.1128/JVI.01304-07.

43. Nakai, H., Fuess, S., Storm, T.A., Muramatsu, S.i., Nara, Y., and Kay, M.A. (2005). Unrestricted hepatocyte transduction with adeno-associated virus serotype 8 vectors in mice. J. Virol. *79*, 214–224. https://doi.org/10.1128/JVI.79.1.214-224.2005.

44. Tomatsu, S., Montaño, A.M., Ohashi, A., Gutierrez, M.A., Oikawa, H., Oguma, T., Dung, V.C., Nishioka, T., Orii, T., and Sly, W.S. (2008). Enzyme replacement therapy in a murine model of Morquio A syndrome. Hum. Mol. Genet. *17*, 815–824. https://doi.org/10.1093/hmg/ddm353.

45. Tomatsu, S., Orii, K.O., Vogler, C., Nakayama, J., Levy, B., Grubb, J.H., Gutierrez, M.A., Shim, S., Yamaguchi, S., Nishioka, T., et al. (2003). Mouse model of N-acetylgalactosamine-6-sulfate sulfatase deficiency (Galns-/-) produced by targeted disruption of the gene defective in Morquio A disease. Hum. Mol. Genet. *12*, 3349–3358. https://doi.org/10.1093/hmg/ddg366.

46. Tomatsu, S., Montaño, A.M., Dung, V.C., Ohashi, A., Oikawa, H., Oguma, T., Orii, T., Barrera, L., and Sly, W.S. (2010). Enhancement of drug delivery: enzyme-replacement therapy for murine Morquio A syndrome. Mol. Ther. *18*, 1094–1102. https://doi.org/10.1038/mt.2010.32.

47. Tomatsu, S., Montaño, A.M., Oikawa, H., Dung, V.C., Hashimoto, A., Oguma, T., Gutiérrez, M.L., Takahashi, T., Shimada, T., Orii, T., and Sly, W.S. (2015). Enzyme replacement therapy in newborn mucopolysaccharidosis IVA mice: early treatment rescues bone lesions? Mol. Genet. Metabol. *114*, 195–202. https://doi.org/10.1016/j.ymgme.2014.05.013.

48. Averill, L.W., Kecskemethy, H.H., Theroux, M.C., Mackenzie, W.G., Pizarro, C., Bober, M.B., Ditro, C.P., and Tomatsu, S. (2021). Tracheal narrowing in children and adults with mucopolysaccharidosis type IVA: evaluation with computed tomography angiography. Pediatr. Radiol. *51*, 1202–1213. https://doi.org/10.1007/s00247-020-04946-0.

49. Doherty, C., Averill, L.W., Theroux, M., Mackenzie, W.G., Pizarro, C., Mason, R.W., and Tomatsu, S. (2018). Natural history of Morquio A patient with tracheal obstruction from birth to death. Mol. Genet. Metab. Rep. *14*, 59–67. https://doi.org/10.1016/j.ymgmr.2017.11.005.

50. Tomatsu, S., Averill, L.W., Sawamoto, K., Mackenzie, W.G., Bober, M.B., Pizarro, C., Goff, C.J., Xie, L., Orii, T., and Theroux, M. (2016). Obstructive airway in Morquio A syndrome., the past., the present and the future. Mol. Genet. Metabol. *117*, 150–156. https://doi.org/10.1016/j.ymgme.2015.09.007.

51. Cleary, M., Davison, J., Gould, R., Geberhiwot, T., Hughes, D., Mercer, J., Morrison, A., Murphy, E., Santra, S., Jarrett, J., et al. (2021). Impact of long-term elosulfase alfa treatment on clinical and patient-reported outcomes in patients with mucopolysaccharidosis type IVA: results from a Managed Access Agreement in England. Orphanet J. Rare Dis. *16*, 38. https://doi.org/10.1186/s13023-021-01675-x.

52. Doherty, C., Stapleton, M., Piechnik, M., Mason, R.W., Mackenzie, W.G., Yamaguchi, S., Kobayashi, H., Suzuki, Y., and Tomatsu, S. (2019). Effect of enzyme replacement therapy on the growth of patients with Morquio A. J. Hum. Genet. *64*, 625–635. https://doi.org/10.1038/s10038-019-0604-6.

53. Lin, H.Y., Chen, M.R., Lin, S.M., Hung, C.L., Niu, D.M., Chuang, C.K., and Lin, S.P. (2018). Cardiac features and effects of enzyme replacement therapy in Taiwanese patients with Mucopolysaccharidosis IVA. Orphanet J. Rare Dis. *13*, 148. https://doi.org/10.1186/s13023-018-0883-6.

54. Fujitsuka, H., Sawamoto, K., Peracha, H., Mason, R.W., Mackenzie, W., Kobayashi, H., Yamaguchi, S., Suzuki, Y., Orii, K., Orii, T., et al. (2019). Biomarkers in patients with mucopolysaccharidosis type II and IV. Mol. Genet. Metab. Rep. *19*, 100455. https://doi.org/10.1016/j.ymgmr.2019.100455.

55. Yabe, H., Tanaka, A., Chinen, Y., Kato, S., Sawamoto, K., Yasuda, E., Shintaku, H., Suzuki, Y., Orii, T., and Tomatsu, S. (2016). Hematopoietic stem cell transplantation for Morquio A syndrome. Mol. Genet. Metabol. *117*, 84–94. https://doi.org/10.1016/j.ymgme.2015.09.011.

56. Chusho, H., Tamura, N., Ogawa, Y., Yasoda, A., Suda, M., Miyazawa, T., Nakamura, K., Nakao, K., Kurihara, T., Komatsu, Y., et al. (2001). Dwarfism and early death in mice lacking C-type natriuretic peptide. Proc. Natl. Acad. Sci. USA *98*, 4016–4021. https://doi.org/10.1073/pnas.071389098.

57. Kake, T., Kitamura, H., Adachi, Y., Yoshioka, T., Watanabe, T., Matsushita, H., Fujii, T., Kondo, E., Tachibe, T., Kawase, Y., et al. (2009). Chronically elevated plasma C-type natriuretic peptide level stimulates skeletal growth in transgenic mice. Am. J. Physiol. Endocrinol. Metab. *297*, E1339–E1348. https://doi.org/10.1152/ajpendo.00272.2009.

58. Komatsu, Y., Chusho, H., Tamura, N., Yasoda, A., Miyazawa, T., Suda, M., Miura, M., Ogawa, Y., and Nakao, K. (2002). Significance of C-type natriuretic peptide (CNP) in endochondral ossification: analysis of CNP knockout mice. J. Bone Miner. Metabol. *20*, 331–336. https://doi.org/10.1007/s007740200048.

59. Tsuji, T., Kondo, E., Yasoda, A., Inamoto, M., Kiyosu, C., Nakao, K., and Kunieda, T. (2008). Hypomorphic mutation in mouse Nppc gene causes retarded bone growth due to impaired endochondral ossification. Biochem. Biophys. Res. Commun. *376*, 186–190. https://doi.org/10.1016/j.bbrc.2008.08.139.

60. Rintz, E., Węgrzyn, G., Fujii, T., and Tomatsu, S. (2022). Molecular Mechanism of Induction of Bone Growth by the C-Type Natriuretic Peptide. Int. J. Mol. Sci. *23*, 5916. https://doi.org/10.3390/ijms23115916.

61. Ueda, Y., Yasoda, A., Hirota, K., Yamauchi, I., Yamashita, T., Kanai, Y., Sakane, Y., Fujii, T., and Inagaki, N. (2019). Exogenous C-type natriuretic peptide therapy for impaired skeletal growth in a murine model of glucocorticoid treatment. Sci. Rep. *9*, 8547. https://doi.org/10.1038/s41598-019-44975-w.

62. Nakao, K., Osawa, K., Yasoda, A., Yamanaka, S., Fujii, T., Kondo, E., Koyama, N., Kanamoto, N., Miura, M., Kuwahara, K., et al. (2015). The Local CNP/GC-B system in growth plate is responsible for physiological endochondral bone growth. Sci. Rep. *5*, 10554. https://doi.org/10.1038/srep10554.

63. Bükülmez, H., Khan, F., Bartels, C.F., Murakami, S., Ortiz-Lopez, A., Sattar, A., Haqqi, T.M., and Warman, M.L. (2014). Protective effects of C-type natriuretic peptide on linear growth and articular cartilage integrity in a mouse model of inflammatory arthritis. Arthritis Rheumatol. *66*, 78–89. https://doi.org/10.1002/art.38199.

64. Lorget, F., Kaci, N., Peng, J., Benoist-Lasselin, C., Mugniery, E., Oppeneer, T., Wendt, D.J., Bell, S.M., Bullens, S., Bunting, S., et al. (2012). Evaluation of the therapeutic potential of a CNP analog in a Fgfr3 mouse model recapitulating achondroplasia. Am. J. Hum. Genet. *91*, 1108–1114. https://doi.org/10.1016/j.ajhg.2012.10.014.

65. Berry, G.E., and Asokan, A. (2016). Cellular transduction mechanisms of adeno-associated viral vectors. Curr. Opin. Virol. *21*, 54–60. https://doi.org/10.1016/j.coviro.2016.08.001.

66. Wu, C., Wu, F., Pan, J., Morser, J., and Wu, Q. (2003). Furin-mediated processing of Pro-C-type natriuretic peptide. J. Biol. Chem. *278*, 25847–25852. https://doi.org/10.1074/jbc.M301223200.

67. Prickett, T.C., and A Espiner, E. (2020). Circulating products of C-type natriuretic peptide and links with organ function in health and disease. Peptides *132*, 170363. https://doi.org/10.1016/j.peptides.2020.170363.

68. Daniels, R.W., Rossano, A.J., Macleod, G.T., and Ganetzky, B. (2014). Expression of multiple transgenes from a single construct using viral 2A peptides in Drosophila. PLoS One *9*, e100637. https://doi.org/10.1371/journal.pone.0100637.

69. Tomatsu, S., Okamura, K., Taketani, T., Orii, K.O., Nishioka, T., Gutierrez, M.A., Velez-Castrillon, S., Fachel, A.A., Grubb, J.H., Cooper, A., et al. (2004). Development and testing of new screening method for keratan sulfate in mucopolysaccharidosis IVA. Pediatr. Res. *55*, 592–597. https://doi.org/10.1203/01.PDR.0000113767.60140.E9.

70. Khan, S.A., Mason, R.W., Giugliani, R., Orii, K., Fukao, T., Suzuki, Y., Yamaguchi, S., Kobayashi, H., Orii, T., and Tomatsu, S. (2018). Glycosaminoglycans analysis in blood and urine of patients with mucopolysaccharidosis. Mol. Genet. Metabol. *125*, 44–52. https://doi.org/10.1016/j.ymgme.2018.04.011.

71. Hendriksz, C.J., Burton, B., Fleming, T.R., Harmatz, P., Hughes, D., Jones, S.A., Lin, S.P., Mengel, E., Scarpa, M., Valayannopoulos, V., et al. (2014). Efficacy and safety of enzyme replacement therapy with BMN 110 (elosulfase alfa) for Morquio A syndrome (mucopolysaccharidosis IVA): a phase 3 randomised placebo-controlled study. J. Inherit. Metab. Dis. *37*, 979–990. https://doi.org/10.1007/s10545-014-9715-6.

72. Hendriksz, C.J., Parini, R., AlSayed, M.D., Raiman, J., Giugliani, R., Solano Villarreal, M.L., Mitchell, J.J., Burton, B.K., Guelbert, N., Stewart, F., et al. (2016). Long-term endurance and safety of elosulfase alfa enzyme replacement therapy in patients with Morquio A syndrome. Mol. Genet. Metabol. *119*, 131–143. https://doi.org/10.1016/j.ymgme.2016.05.018.

73. Tomatsu, S., Montaño, A.M., Oguma, T., Dung, V.C., Oikawa, H., de Carvalho, T.G., Gutiérrez, M.L., Yamaguchi, S., Suzuki, Y., Fukushi, M., et al. (2010). Validation of keratan sulfate level in mucopolysaccharidosis type IVA by liquid chromatography-tandem mass spectrometry. J. Inherit. Metab. Dis. *33*, S35–S42. https://doi.org/10.1007/s10545-009-9013-x.

74. Takahashi, K., Tanabe, K., Ohnuki, M., Narita, M., Ichisaka, T., Tomoda, K., and Yamanaka, S. (2007). Induction of pluripotent stem cells from adult human fibroblasts by defined factors. Cell *131*, 861–872. https://doi.org/10.1016/j.cell.2007.11.019.

75. Szymczak, A.L., Workman, C.J., Wang, Y., Vignali, K.M., Dilioglou, S., Vanin, E.F., and Vignali, D.A.A. (2004). Correction of multi-gene deficiency *in vivo* using a single 'self-cleaving' 2A peptide-based retroviral vector. Nat. Biotechnol. *22*, 589–594. Erratum in: Nat Biotechnol. 22(12):1590. Erratum in: Nat Biotechnol. 2004 Jun;22(6):760. https://doi.org/10.1038/nbt957.

76. Vaseghi, H.R., Yin, C., Zhou, Y., Wang, L., Liu, J., and Qian, L. (2016). Generation of an inducible fibroblast cell line for studying direct cardiac reprogramming. Genesis *54*, 398–406. https://doi.org/10.1002/dvg.22947.

77. Tang, W., Ehrlich, I., Wolff, S.B.E., Michalski, A.M., Wölfl, S., Hasan, M.T., Lüthi, A., and Sprengel, R. (2009). Faithful expression of multiple proteins via 2A-peptide self-processing: a versatile and reliable method for manipulating brain circuits. J. Neurosci. *29*, 8621–8629. https://doi.org/10.1523/JNEUROSCI.0359-09.2009.

78. Verrier, J.D., Madorsky, I., Coggin, W.E., Geesey, M., Hochman, M., Walling, E., Daroszewski, D., Eccles, K.S., Ludlow, R., and Semple-Rowland, S.L. (2011).

Bicistronic lentiviruses containing a viral 2A cleavage sequence reliably co-express two proteins and restore vision to an animal model of LCA1. PLoS One *6*, e20553. https://doi.org/10.1371/journal.pone.0020553.

79. Geier, M., Fauland, P., Vogl, T., and Glieder, A. (2015). Compact multi-enzyme pathways in P. pastoris. Chem. Commun. *51*, 1643–1646. https://doi.org/10.1039/c4cc08502g.

80. Liu, Z., Chen, O., Wall, J.B.J., Zheng, M., Zhou, Y., Wang, L., Vaseghi, H.R., Qian, L., and Liu, J. (2017). Systematic comparison of 2A peptides for cloning multi-genes in a polycistronic vector. Sci. Rep. *7*, 2193. https://doi.org/10.1038/s41598-017-02460-2.

81. Woods, A., Khan, S., and Beier, F. (2007). C-type natriuretic peptide regulates cellular condensation and glycosaminoglycan synthesis during chondrogenesis. Endocrinology *148*, 5030–5041. https://doi.org/10.1210/en.2007-0695.

82. Yamashita, T., Fujii, T., Yamauchi, I., Ueda, Y., Hirota, K., Kanai, Y., Yasoda, A., and Inagaki, N. (2020). C-Type Natriuretic Peptide Restores Growth Impairment Under Enzyme Replacement in Mice With Mucopolysaccharidosis VII. Endocrinology *161*, bqaa008. https://doi.org/10.1210/endocr/bqaa008.

83. Geisler, A., and Fechner, H. (2016). MicroRNA-regulated viral vectors for gene therapy. World J. Exp. Med. *6*, 37–54. https://doi.org/10.5493/wjem.v6.i2.37.

84. Qiao, C., Yuan, Z., Li, J., He, B., Zheng, H., Mayer, C., Li, J., and Xiao, X. (2011). Liver-specific microRNA-122 target sequences incorporated in AAV vectors efficiently inhibits transgene expression in the liver. Gene Ther. *18*, 403–410. https://doi.org/10.1038/gt.2010.157.

85. Sosa, A.C., Kariuki, B., Gan, Q., Knutsen, A.P., Bellone, C.J., Guzmán, M.A., Barrera, L.A., Tomatsu, S., Chauhan, A.K., Armbrecht, E., and Montaño, A.M. (2020). Oral immunotherapy tolerizes mice to enzyme replacement therapy for Morquio A syndrome. J. Clin. Invest. *130*, 1288–1300. https://doi.org/10.1172/JCI125607.